J. Phys. D: Appl. Phys. **33** (2000) R247–R268. Printed in the UK PII: S0022-3727(00)09438-9

TOPICAL REVIEW

# Mechanisms for exchange bias

**R L Stamps**

Department of Physics, University of Western Australia, Nedlands WA 6907, Australia

E-mail: stamps@physics.uwa.edu.au

Received 6 October 2000

**Abstract.** Modern applications for thin film magnets involve unique requirements for the control and design of specific magnetic properties. The exchange bias effect in ferromagnet/antiferromagnet bilayers appears to be a useful feature for controlling one of the most important characteristics of a ferromagnet: coercivity. Prospects for control and enhancement of desirable effects depend upon a clear understanding of mechanisms governing exchange bias. The processes underlying the existence and properties of exchange bias are reviewed, with particular emphasis on the roles of interface structure and temperature. Results from numerical simulations are used to illustrate how exchange bias is modified by geometric structures at the interface and randomly placed defects. A general theoretical formulation of the bias problem is proposed, and an expression for the interface energy is derived. A key result is the existence of higher-order coupling terms when more than one sublattice of the antiferromagnet is present at the interface. Results from calculations of finite temperature effects on bias and coercivity are described, and the concept of viscosity in the antiferromagnet is discussed. A brief discussion is also included of how a dynamic linear response, such as ferromagnetic resonance or light scattering, can be used to determine relevant anisotropy and exchange parameters.

## 1. Introduction

Much research into thin film magnetism over the past fifteen years has been driven by important and useful features associated with interfaces involving magnetic materials. A well known achievement of this research has been the development and application of giant magnetoresistance. Since then, a new technology has emerged, 'spin electronics'; an area that has seen remarkable growth in recent years. The integration of magnetic structures with semiconductor technology on a nanoscopic scale is a goal currently pursued with great vigour, particularly for applications in data storage and sensing device technologies. A general introduction to the topic has been given by Prinz (1995).

The key to the successful design of magnetic structures for application is the ability to manipulate and control magnetic properties. The basic energies involved are exchange and anisotropy, where the former controls magnetic ordering and the latter controls the preferred orientation. Both are phenomenological descriptions of fundamental correlations and energies associated with the electronic and crystalline structure of a material. A powerful technique for modifying and controlling magnetic characteristics is based on the use of magnetic heterostructures with properties governed by the interface region.

One of the most interesting interfaces for basic study and application is the interface between a ferromagnet and an antiferromagnet. A ferromagnet, such as iron, has a large exchange parameter but a relatively small anisotropy. This makes ferromagnetic order stable at high temperatures but the orientation may not be, particularly if the dimensions are a few nanometres. Many antiferromagnets have large anisotropies and consequently very stable orientations. In heterostructures, exchange coupling between the ferromagnet and antiferromagnet can, in principle, produce a ferromagnetic behaviour with stable order and high anisotropy. In such a structure, the anisotropy may behave as uni-directional—a feature not found in ferromagnets. This phenomena is called exchange bias because the hysteresis loop associated with the ferromagnet/antiferromagnet structure can be centred about a non-zero magnetic field.

The phenomena of exchange bias is a topic that has been visited and revisited several times over the past forty years, beginning with Meiklejohn and Bean (1956) and Jacobs and Bean (1966). The reason is that there is an inherent complexity in a structural combination that leads to competing interactions. This is precisely what happens at an interface where both ferromagnetic and antiferromagnetic interactions can compete for magnetic order. The presence of strong local anisotropies can also contribute, with the result of unusual reversible and irreversible processes governing the magnetization and static susceptibility. It has been suggested that some aspects of the magnetic behaviour may be closely related to those observed in disordered magnets and spin glasses (Malozemoff 1988, Schlenker *et al* 1986, Kouvel 1963).

  

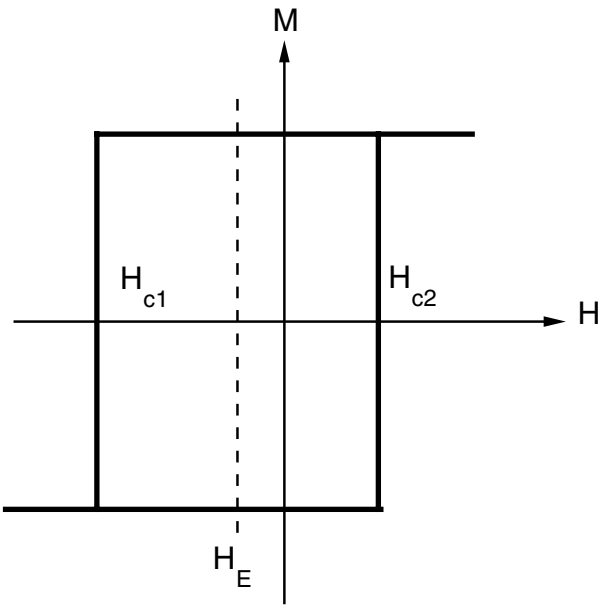


**Figure 1.** Shifted hysteresis in an exchange biased ferromagnet. Characteristic fields are the bias, $H_E$, and coercivities, $H_{c1}$ and $H_{c2}$.

### 1.1. Applications and relevant features

An example shifted hysteresis is sketched in figure 1. The centre of the hysteresis loop is shifted from zero applied magnetic field by an amount $H_E$, the exchange bias field. There are three different fields used to characterize the bias: the left and right coercive fields, $H_{c1}$ and $H_{c2}$, and the bias field.

One application for exchange bias is to 'pin' the ferromagnet along a particular direction. If the applied field strength is less than $H_{c1}$, for example, then the ferromagnet will not reverse. This feature is of interest for applications in spin valves and magnetic tunnel junctions. Furthermore, because the interface exchange provides a means for anisotropies in the antiferromagnet to affect magnetic order in the ferromagnet, exchange bias is also of interest in terms of 'anisotropy engineering'. This is relevant, for example, for modifying activation energies and volumes in fine particles (Fulcomer and Charap 1972, van der Heijden *et al* 1998b).

Relevant characteristics of the bias and coercivity fields are immediately apparent. In terms of magnitude and design, the sensitivity and dependence of the fields to interface structure and quality are important. Stability to magnetic field and thermal fluctuations is also a significant issue. Long-term stability for the magnitude of the bias field and orientation of the ferromagnet can also be important. Of particular interest for design applications is the degree to which the bias and coercive fields can be adjusted through film thickness, growth conditions and choice of materials.

### 1.2. Proposed mechanisms

In the light of the above considerations, experimental studies of exchange bias have presented a number of puzzles and contradictions. Of these, the most serious has been an inability for models of exchange bias to correctly predict the magnitude of the bias or coercive fields. This was recognized quite early, and led to the recognition of a number of processes possibly involved in exchange bias (Néel 1967).

These additional considerations fall mostly into two categories. The first is the recognition that reorientation of the ferromagnet through application of an applied magnetic field can require formation of magnetic domain wall structures on either side of the interface (Mauri *et al* 1987, Koon 1997, Schulthess and Butler 1998, Stiles and McMichael 1999a, Camley *et al* 1999, Kiwi *et al* 1999b). The second category was defined early on, with considerations of domain formation and domain wall motion, pinning and de-pinning during reversal of the ferromagnet (Meiklejohn 1962, Schlenker and Paccard 1967, Schlenker 1968a, 1968b, Néel 1988). Since then, theories have been put forward that describe domain and wall dynamics in the antiferromagnet (Malozemoff 1987, Nemoto *et al* 1999, Nikitenko *et al* 2000, Kiwi *et al* 1999a), and also domain dynamics in the ferromagnet component (Li and Zhang 2000, Kiwi *et al* 1999a, Leighton *et al* 2000).

Because the exchange bias is intimately connected with details of the magnetization process during reversal and the subsequent formation of hysteresis, considerations of time dependence and irreversible processes are also relevant (Schlenker 1968b, Fulcomer and Charap 1972, Schlenker *et al* 1986). This has led to a number of more recent examinations of thermal effects (van der Heijden *et al* 1998a, 1998b, Gökemeijer *et al* 1999, Farrow *et al* 1997). Magnetic viscosity experiments have also been reported, including field rate studies (Geoghegan *et al* 1998, Goodman *et al* 1999, 2000). The importance of thermal processes on exchange bias and coercivity means that the magnetization history is important (Miltényi *et al* 1999, Nogués *et al* 2000b), and can result in a variety of curious behaviours including positive exchange bias (Nogués *et al* 1996, 2000a).

There are many interesting results appearing from experiments that provide challenges and testing grounds for models of exchange bias mechanisms. One class of these experiments is rotational hysteresis and torque measurements. This technique was used quite early as a natural way of measuring the uni-directional anisotropy and is still valuable (Meiklejohn 1962, Schlenker 1968b, Tsunoda *et al* 2000). There is a wealth of information available from the analysis of spatial correlations during the magnetization process that can be obtained from scanning probe studies of domain formation and dynamics (Nikitenko *et al* 1998, Kiwi *et al* 1999a, Fitzsimmons *et al* 2000). Ferromagnetic resonance and light scattering studies of linear response also offer unique views of exchange bias materials (McMichael *et al* 1998, Mathieu *et al* 1998, Ercole *et al* 2000). Nonlinear dynamic experiments are also possible and may provide particularly interesting results on nonequilibrium processes on short timescales (Ju *et al* 1999).

### 1.3. Outline

The emerging picture of mechanisms for exchange bias is complicated by the dynamics of interface spins frustrated by competing interactions. In order to provide a reasonably coherent picture of the current state of understanding, the

following discussion is organized somewhat along historical lines. In section 2, one of the initial, and simplest, models of exchange bias is described, and useful empirical definitions for uni-directional anisotropy fields are presented. Next, based on general energy considerations, refinements are argued for with the introduction of a 'partial wall' picture. This leads naturally to a consideration of interface structure and the question of imperfections discussed in section 3. Stability requirements for exchange bias with mixed sublattice interfaces are examined, and results from numerical simulations on systems with structured interfaces are described.

A theory of exchange bias is constructed in section 4 in order to justify the use of proposed models of the interface energy, and to provide a means of defining useful parameters for the interface region. The idea of stability is further examined in terms of thermal processes and effects in section 5 in the context of mean field theory and also using Monte Carlo simulations for time-dependent effects. Section 6 contains a brief summary of linear response dynamics, with a particular focus on how resonance and light scattering can be used to obtain measures of interface parameters governing the exchange bias. The main points and conclusions are summarized in section 7.

The mechanisms discussed in the following sections are based on semi-classical theories of magnetization processes. Interesting alternative formulations have also been explored using magnon theory, but these will not be discussed here (Suhl and Schuller 1998, Hong 1998). The discussion is limited to exchange bias effects involving ferromagnets and naturally occurring antiferromagnets, although it is noted that combinations involving 'artificial' antiferromagnets can also display bias shifts (Jiang *et al* 2000). Also, no attempt has been made to survey the experimental literature. The reader is instead referred to excellent reviews by Nogués *et al* (1999) and Berkowitz and Takano (1999).

## 2. Basic mechanisms for perfect interfaces

A shifted hysteresis, such as that sketched in figure 1, can be obtained experimentally in the following way. First, a magnetic field is applied in order to saturate the ferromagnet in the field direction. This is done at a temperature above the ordering temperature $T_N$ of the antiferromagnet. The second step is to cool the sample below $T_N$ while in the field. A shift in the hysteresis loop can appear if measured after cooling.

### 2.1. Rigid antiferromagnet model

Meiklejohn and Bean (1956, 1957) suggested that this shift is due to a large anisotropy in the antiferromagnet and a weaker exchange energy coupling the ferromagnet and antiferromagnet. A schematic diagram of the process is given in figure 2 for a ferromagnet with no anisotropy. In figure 2($a$), the saturating magnetic field is applied for a temperature above $T_N$. This aligns the ferromagnet, and after cooling the system while still in the field, the magnetization remains pinned along the original direction for small negative fields, as in figure 2($b$). A field large enough to overcome the interlayer exchange reverses the ferromagnet, as shown in figure 2($c$). On the reverse path, the ferromagnet rotates back into the original positive direction while the applied field is still negative. This gives a shifted magnetization curve as shown in figure 1. The magnitude of the shift is equal to the effective field associated with the interlayer exchange.

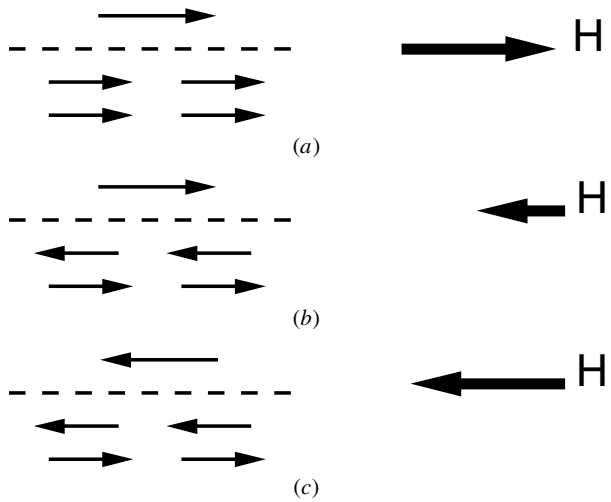


**Figure 2.** Meiklejohn and Bean mechanism for bias. In ($a$), a saturating magnetic field is applied in order to align the ferromagnet above $T_N$. After cooling the system in field, the magnetization remains pinned along the original direction when the field is reversed as shown in ($b$). A sufficiently large field reverses the ferromagnet in ($c$).

A hysteretic loop appears when anisotropy is included in the ferromagnet. Bounds for the coercive fields, $H_{c1}$ and $H_{c2}$, can be found by examining the stability of a model energy of the form

$$E = -HMt_f \cos\theta - J\cos\theta + K_f \sin^2\theta. \qquad (1)$$

In this model, the applied magnetic field is $H$, $M$ is the saturation magnetization of the ferromagnet, $t_f$ is the thickness of the ferromagnetic film, $J$ is the interlayer exchange between the ferromagnet and the antiferromagnet, and $K_f$ is a uniaxial anisotropy in the ferromagnet. The angle $\theta$ is taken between $M$ and the uniaxial anisotropy easy axis. The field is aligned along the easy axis and the magnetization is assumed to remain uniform in this model. The most important restriction is that the antiferromagnet remains rigidly aligned along the direction of its easy axis, assumed to also lie parallel to the ferromagnet easy axis.

The energy has extrema corresponding to saturation in the $\theta = 0$ and $\pi$ directions. Stability of the $\theta = 0$ configuration is possible if $J + H + 2K_f > 0$, and stability of the $\theta = \pi$ configuration is possible if $2K_f - J - H > 0$. This corresponds to coercive fields

$$H_{c1} = -\frac{2K_f + J}{Mt_f} \qquad (2)$$

and

$$H_{c2} = \frac{2K_f - J}{Mt_f}. \qquad (3)$$

Because the coercive fields are not equal in magnitude, the entire hysteresis is biased. The bias field in this model can

be defined as the midpoint of the hysteresis and is directly proportional to the exchange coupling:

$$H_{\mathrm{E}} = \frac{J}{Mt_{\mathrm{f}}}. \tag{4}$$

Note that the bias field is determined by competition between the Zeeman energy and the interlayer exchange energy, and therefore depends on the thickness of the ferromagnet.

It is useful to also note that the bias can be interpreted as an exchange coupled anisotropy field acting on the ferromagnet. The effective magnetic field acting on the ferromagnet is defined as

$$H_{\mathrm{f}} = -\frac{1}{M}\nabla_f E. \tag{5}$$

A notation defined in equation (5) will be used in later sections and is the definition of $\boldsymbol{f}$ as a unit vector in the direction of the ferromagnet magnetization. This results in the equivalence

$$\cos\theta = \boldsymbol{f}\cdot\boldsymbol{n}_{\mathrm{f}} \tag{6}$$

where $\boldsymbol{n}_{\mathrm{f}}$ is a unit vector defined in the direction of the ferromagnetic easy axis.

Equation (5) applied to the energy in equation (1) gives

$$\vec{H}_{\mathrm{eff}} = -\frac{2K_{\mathrm{f}}}{M}\boldsymbol{f} + (H + H_{\mathrm{E}})\boldsymbol{n}_{\mathrm{f}}. \tag{7}$$

The first term represents the ferromagnet anisotropy fields, but the third term is sometimes thought of as a contribution from a uni-directional anisotropy of magnitude $J/Mt_{\mathrm{f}}$.

### 2.2. Partial wall model of the uncompensated interface

The remainder of this article is in some sense an extended footnote to equation (7) detailing the various corrections involved when considering exchange bias in thin film magnetic multilayers. The first correction has been noted by several authors, and is the recognition that a perfectly rigid antiferromagnet, and a perfectly uniform ferromagnet, may not properly describe the lowest energy magnetic configuration near the interface (Néel 1967, Mauri *et al* 1987, Koon 1997, Kiwi *et al* 1999b). This point will be examined in detail in section 4 but, for the moment, an intuitive argument serves to illustrate the basic idea.

Consider a long chain of $N$ magnetic moments with nearest neighbour ferromagnetic exchange coupling and a uniaxial anisotropy energy. A configuration with the moments at one end rotated 180° from the moments at the other end will have an energy that depends on how the rotation occurs. Suppose at each end the moments are aligned along the easy axis in the positive $z$ direction. If a magnetic domain wall is formed, then neglecting magnetostatic contributions, the energy of the twist will be proportional to $\sqrt{J_{\mathrm{f}}K_{\mathrm{f}}}$ where $J$ is the exchange integral of the ferromagnetic chain. The energy of this configuration is less than the energy needed to align half of the moments along the $+z$ direction and half along the $-z$ direction.

Now consider an exchange bias structure as a long chain of $N$ ferromagnetically coupled moments and $N$ antiferromagnetically coupled moments. The moments at the interface are connected by an exchange energy $J_1$. According to the above argument, the configuration sketched in figure 2($c$) should be higher in energy than a configuration in which the ferromagnet and antiferromagnet moments form some type of twist. This means that the bias field given by equation (4) is too large by an amount related to the energy of a domain wall at the interface.

In general, it is energetically favourable to build a twist into a magnetic chain by distributing the twist over a number of moments. However, it is not always possible to form a stable twist configuration near or across an interface. One of the main points of this article is that this feature is a main factor controlling exchange bias shifts and coercive fields.

Expressions for the bias field with a twist formed in the antiferromagnet can be derived by including the energy of a twist into the energy of the coupled ferromagnet/antiferromagnet system. An uncompensated interface with only one antiferromagnet sublattice is considered first. Defining the vectors $\boldsymbol{a}$ and $\boldsymbol{n}_{\mathrm{af}}$ for the direction of the interface antiferromagnet moment and the antiferromagnet easy axis, respectively, the total energy of the uncompensated system is

$$E_{\mathrm{u}} = -\boldsymbol{H}Mt_{\mathrm{f}}\cdot\boldsymbol{f} + J_1\boldsymbol{f}\cdot\boldsymbol{a} + \sigma(1 - \boldsymbol{a}\cdot\boldsymbol{n}_{\mathrm{af}}). \tag{8}$$

This energy is written for arbitrary orientation of the applied field $\boldsymbol{H}$, and assumes no anisotropy in the ferromagnet. The ferromagnet is assumed to rotate rigidly without forming a significant twist. This is a reasonable assumption for thin ferromagnet films with large exchange and small anisotropies. The conditions for a twist formed in the ferromagnet will be considered in section 4.

The bias field is defined here as the magnitude of $\boldsymbol{H}$ necessary to align the ferromagnet perpendicular to the applied field such that $\boldsymbol{H}\cdot\boldsymbol{f} = 0$. This can be found easily from the effective field calculated from the energy of equation (8) using equation (5). In terms of an angle $\rho$ specifying the direction of the applied magnetic field $\boldsymbol{H}$ measured relative to the antiferromagnet easy axis, the bias field is given by

$$H_{\mathrm{E}} = \frac{J_1}{Mt_{\mathrm{f}}}\frac{\cos\theta}{\sqrt{1 + \frac{J_1}{2\sigma}|\sin\theta| + \left(\frac{J_1}{2\sigma}\right)^2}}. \tag{9}$$

There are several interesting features of this model. Firstly, and most importantly, the magnitude of the bias field is reduced by the formation of a twist in the antiferromagnet. This is seen most clearly by considering the special case of the field aligned along the antiferromagnet easy axis ($\rho = 0$):

$$H_{\mathrm{E}} = \frac{J_1}{Mt_{\mathrm{f}}\sqrt{1 + \left(\frac{J_1}{2\sigma}\right)^2}}. \tag{10}$$

The twist energy is an important correction to the magnitude, as noted by Mauri *et al* (1987). The magnitude of the correction can be estimated by noting that $J_1/\sigma$ has the form of a domain wall length in units of atomic layers. If $J_1$ is of the order of magnitude of the antiferromagnet exchange, then this length will be around ten layers. This reduces $H_{\mathrm{E}}$ by an order of magnitude from the untwisted

bias result of equation (4). An interesting consequence is that the antiferromagnet must be thick enough to support partial wall formation. This leads to a dependence of the bias field on the thickness of the antiferromagnet. Dependence on antiferromagnet thickness of the bias field antiferromagnet has been observed in several experiments (Allegranza and Chen 1993, van Driel *et al* 2000, Xi and White 2000a).

The second important feature of equation (9) is that the bias field is largest for directions along the antiferromagnet easy axis, and zero for directions perpendicular to the easy axis. This will be seen to be of particular importance in section 3 when examining the effect of interface structure on the bias field and properties. It is interesting to note that the $\theta$ dependence of the bias field can be described by a few terms in a cosine or sine expansion (Ambrose and Chien 1994, Ambrose *et al* 1997). The angular dependence provides information about the nature of the interface, and is one means of characterizing imperfect interfaces (Wu and Chien 1998, Dimitrov *et al* 1998, Tang *et al* 1999, Xi and White 1999, Xi *et al* 1999a, Kim *et al* 2000).

The shape of the magnetization curve is also revealing and can be determined by minimizing the energy of equation (8). A way of locating a minimum energy configuration is to require the torques

$$\boldsymbol{\Gamma}_{\mathrm{f}} = \boldsymbol{f} \times \boldsymbol{H}_{\mathrm{f}} \tag{11}$$

and

$$\boldsymbol{\Gamma}_{\mathrm{af}} = \boldsymbol{a} \times \boldsymbol{H}_{\mathrm{a}} \tag{12}$$

to vanish and to check that the corresponding configuration is actually a stable minimum of the energy. The effective field $\boldsymbol{H}_{\mathrm{a}}$ is defined for the antiferromagnet vector $\boldsymbol{a}$ in direct analogy to equation (5) for the ferromagnet. The starting point for the calculation is important, and is taken from the solution at the previous field value when calculating a hysteresis loop. A loop calculation is usually begun at saturation.

An example magnetization curve produced by the partial wall mechanism is shown in figure 3. The calculation was performed by minimizing equation (8) as described above, and the projection of the ferromagnet magnetization along the applied field direction is shown as a function of the applied field. The units are reduced with the magnetization given as $m/M = \cos\theta$ and the field as $HMt_{\mathrm{f}}/\sigma$.

Throughout this article, the exchange parameters are given in units of $\sigma$. The value used for figure 3 is $J_1 = 1$. There is no hysteresis because there is no anisotropy in the ferromagnet, and no unstable configurations for this field range in the antiferromagnet. Note the asymptotic approach to saturation for large negative field. This corresponds to the formation of an *almost* 180° domain wall in the antiferromagnet. A full 180° wall cannot exist unless it penetrates into the ferromagnet across the interface, and in fact may not be stable depending on anisotropy and exchange parameters. Instabilities of partial wall formation will be discussed in more detail in section 3, but the consequence is simply that the reversible bias effect will disappear if the applied field is increased beyond a certain value. This point has been discussed by Stiles and McMichael (1999a) and Stamps (2000), and is central to the idea of a 'natural angle' suggested by Camley *et al* (1999).

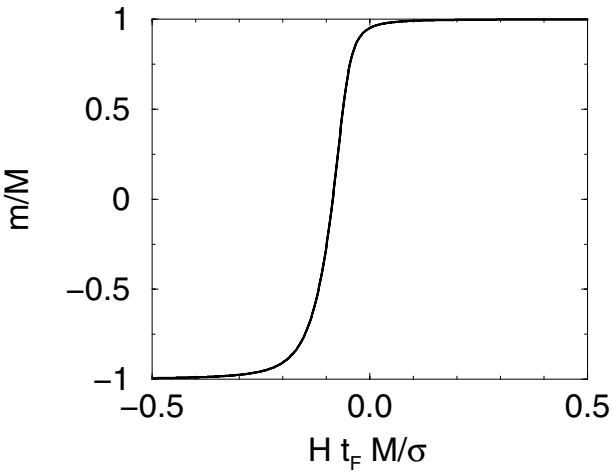


**Figure 3.** Magnetization along the direction of an applied magnetic field as a function of the field for an exchange biased structure. The interface has only one antiferromagnet sublattice present (uncompensated) and $J_1 = 1$. There is no anisotropy in the ferromagnet, and the bias involves a twist formed in the antiferromagnet. Note the asymptotic approach to saturation for negative field.

### 2.3. Magnetic configurations for the compensated interface

A large number of possible interface structures are compensated or partially compensated in that multiple antiferromagnet sublattices may be present and couple to the ferromagnet. This is clearly also possible with disorder present at the interface. The consequences on exchange bias are many, and will be described at length in the following sections. The extreme case of full compensation for an interface between a ferromagnet and a two sublattice antiferromagnet is considered first.

Full compensation means equal fractions of both sublattices are present at the interface, as illustrated in figure 4(*b*). The ferromagnet is then exchange coupled equally to both sublattices. If the antiferromagnet moments are rigidly antiparallel in the interface plane, there is no net moment for the ferromagnet to interact with. The result is that all orientations of the ferromagnet with respect to the antiferromagnet have the same energy. The conclusion is that there can be no exchange bias effect without a net antiferromagnetic moment at the interface.

Based on results of numerical simulations, Koon (1997) suggested that exchange coupling to a ferromagnet at a compensated interface could automatically generate a small magnetic moment through a spontaneous canting of antiferromagnetic spins. The idea is that spins in the interface region are frustrated by competing antiferromagnetic exchange between the two sublattices and the ferromagnet. The competition results in a canted configuration where the spins deviate slightly from the easy axis direction in such a way as to generate a net magnetic moment. The ferromagnet aligns antiparallel to this moment, and consequently orientates perpendicular to the antiferromagnet easy axis. The resulting configuration is sketched in figure 4(*c*).

The feature of perpendicular orientation of the ferromagnet relative to the antiferromagnet easy axis is

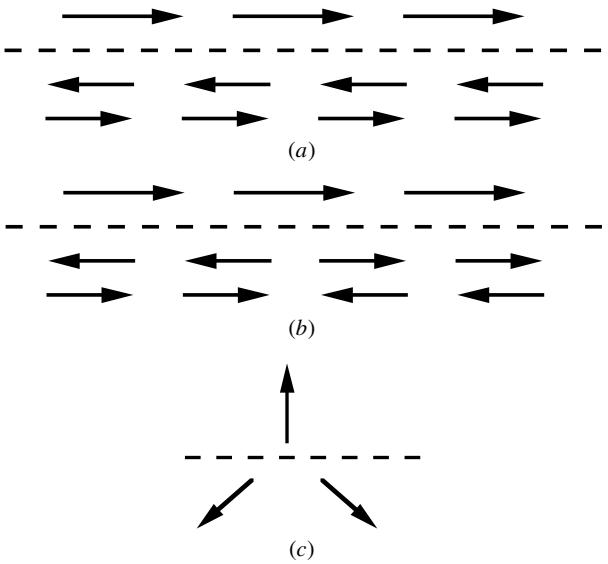


**Figure 4.** Schematic structure of a two sublattice antiferromagnet at (*a*) an uncompensated interface and (*b*) a fully compensated interface. Spin canting at a compensated interface is illustrated in (*c*).

closely related in principle to the idea of biquadratic coupling. In a model by Slonczewski (1991), variations in the sign of coupling along an interface between two ferromagnetic films were shown to result in a perpendicular orientation of the films.

An energy describing this form depends on the square of the cosine of the angle between the two films, and has been suggested to approximate the effect of coupling at a compensated ferromagnet/antiferromagnet interface (Stiles and McMichael 1999a, Stamps 2000). A modified version of equation (8) includes this biquadratic term:

$$E_{\text{inter}} = -\boldsymbol{H}Mt_{\text{f}}\cdot\boldsymbol{f}+J_1\boldsymbol{f}\cdot\boldsymbol{a}+J_2(\boldsymbol{f}\cdot\boldsymbol{a})^2+\sigma(1-\boldsymbol{a}\cdot\boldsymbol{n}_{\text{af}}). \quad (13)$$

The perpendicular coupling appears in the $J_2$ term. In section 4, this energy will be derived from a general argument and shown to be a second-order term in the exchange coupling between a ferromagnet and a canted antiferromagnet. It is the only term that appears when the interface is fully compensated. The $J_2$ contribution to the coupling also involves a number of stability conditions that will be discussed in section 3.

The method used above to derive an expression for the bias field can also be used in this case. If the applied field is aligned perpendicular to the antiferromagnet easy axis, the bias field turns out to be

$$H_{\text{E}} = \frac{\sigma}{2t_{\text{F}}M}\sqrt{1-\left(\frac{\sigma}{4J_2}\right)^2}. \quad (14)$$

Note that a bias field does not exist for all values of the exchange coupling $J_2$. The exchange must satisfy $J_2 > \sigma$ which means that the interface exchange must be larger than the energy required to form a wall in the antiferromagnet. The reason is that a partial wall mechanism for bias in the case of a compensated interface requires that the canting of interfacial spins be preserved through large angle rotations

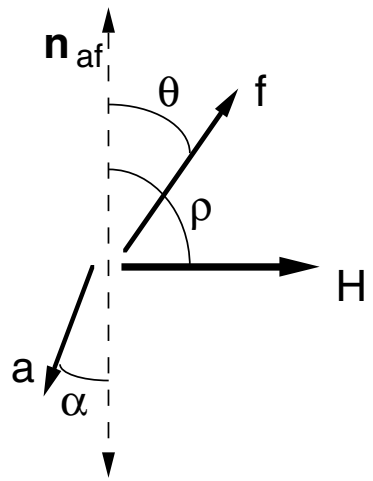


**Figure 5.** Angles for the applied field, ferromagnet, and antiferromagnet defined in reference to the antiferromagnet uniaxial anisotropy axis $\boldsymbol{n}_{\text{af}}$.

of the ferromagnet. This turns out to be possible only by forming a stable domain wall in the antiferromagnet while keeping the ferromagnet mostly aligned with the canted moment. The exchange coupling must therefore be large enough to preserve the relative orientation of the ferromagnet and antiferromagnet interface moments during the entire reversal process.

Before turning to the problem of exchange bias at general interfaces, mention should also be made of another type of partial wall model proposed by Kiwi (1999b). The argument is that exchange bias may be possible at a compensated interface if canting is present, but if the partial wall is formed in the ferromagnet as opposed to the antiferromagnet. Kiwi's calculations suggest that magnitudes for $H_{\text{E}}$ comparable to observed values are possible in this model. This mechanism will be examined again at the end of section 4.

## 3. Stability, interface structure and defects

General features of the exchange bias were described in the previous section for perfect compensated and uncompensated interfaces. In order to discuss exchange bias at partially compensated interfaces, it is first necessary to examine another important issue: stability (Schulthess and Butler 1998, Camley *et al* 1999, Kim *et al* 1999, Stiles and McMichael 1999a).

Considerations for stability were mentioned early in section 2 with regard to coercivity for the rigid antiferromagnet model. A more general description of coercivity is now given in terms of partial wall formation. However, a basic distinction appears. In the rigid antiferromagnet model, the coercivity depended on anisotropies intrinsic to the ferromagnet. Here it will be shown that anisotropy in the ferromagnet is not necessary for coercivity observed in exchange biased structures.

### 3.1. Energy barriers to partial wall formation

The formation of energy barriers is a useful way of understanding the process of ferromagnet reversal with

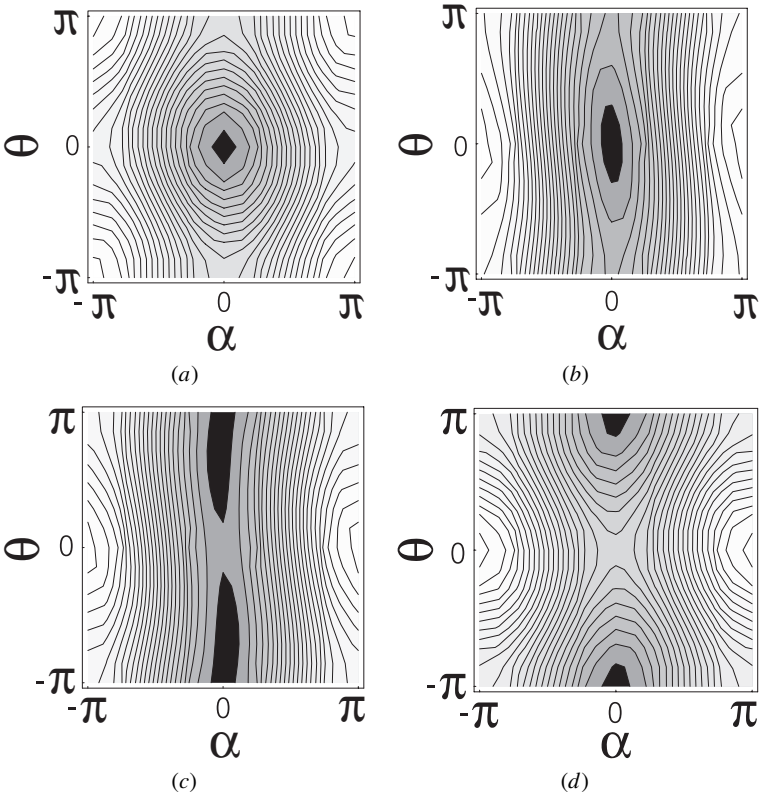


**Figure 6.** Energy contour plots for reversal of the ferromagnet in an applied magnetic field. The horizontal axis is the angle describing the orientation of the antiferromagnet, $\alpha$, and the vertical axis is the angle describing the orientation of the ferromagnet, $\theta$, as defined in figure 5. The interface is uncompensated with $J_1 = 0.1$ and $J_2 = 0.01$. The applied field is aligned along $\rho = 0$ with magnitude $HMt_f/\sigma = 0.5$ in ($a$), $HMt_f/\sigma = 0$ in ($b$), $HMt_f/\sigma = -0.12$ in ($c$) and $HMt_f/\sigma = -0.5$ in ($d$). The darkest regions have the lowest energy.

exchange bias in the partial wall model (Stamps 2000). There are at least two types of barrier important to consider. The first are barriers involved for rotation of magnetization in the plane of the interface, and the second are barriers related to out-of-plane rotation of the magnetizations. In-plane rotation processes are considered first for uncompensated, compensated and partially compensated interfaces.

To understand how in-plane barriers affect exchange bias, it is useful to examine the energies of various magnetic configurations described by equation (13) for different values of the exchange parameters. In section 4, arguments will be presented to show that the energy in equation (13) describes an uncompensated interface if $J_1 \gg J_2$ and a compensated interface if $J_1 = 0$. It will also be argued that a partially compensated (or 'mixed') interface is described when $J_1$ is comparable to $J_2$.

To begin, consider exchange bias for an uncompensated interface. The energy of a magnetic configuration can be conveniently specified in the above model by defining angles shown in figure 5. The angle $\alpha$ specifies the orientation of $\boldsymbol{a}$, and $\theta$ describes the orientation of $\boldsymbol{f}$.

A contour plot of energy calculated from equation (13) is shown in figure 6. The exchange parameters are $J_1 = 0.1$ and $J_2 = J_1^2$ so that $J_1 \gg J_2$. The horizontal axis is the angle describing the orientation of the antiferromagnet, $\alpha$, and the vertical axis is the angle describing the orientation of the ferromagnet, $\theta$. The applied field is aligned along $\theta = 0$.

The applied field is $HMt_f/\sigma = 0.5$ in figure 6($a$), and corresponds to the field cooling direction. There is a single, well defined potential well at $\theta = \alpha = 0$. The well lengthens in the $\theta$ direction as the field is reduced. This is seen in figure 6($b$) where $H = 0$. The well lengthens and splits into two separate wells as the field is made negative. The minima are at non-zero $\alpha$ values so that a small twist exists in the antiferromagnet. At $HMt_f/\sigma = -0.12$, shown in figure 6($c$), there are two distinct wells near $\theta = \pi/2$ and $3\pi/2$. The wells separate, moving towards $\theta = \pi$ and $-\pi$ as the field becomes more negative. This is shown in figure 6($d$) for $HMt_f/\sigma = -0.5$. The magnetization process is reversible as the field is made positive again. This means a shifted magnetization curve and stable bias.

If the partial wall is stable to out-of-plane fluctuations, there is no minimum value of $J_1$ necessary for bias. The case of fully compensated interfaces is very different, as discussed in the previous section where it was found that a minimum value of $J_2$ is necessary for reversible bias to exist. Energy contours for a compensated interface are shown in figure 7 for $J_1 = 0$ and $J_2 = 0.04$. The applied field is applied perpendicular to the antiferromagnet anisotropy axis with $\rho = \pi/2$. At $HMt_f/\sigma = 0.05$ in figure 7($a$), a deep well is at $\theta/2$ and is taken as the cooling direction. A well begins to form at $\theta = 3\pi/2$ as the field is reduced. At $HMt_f/\sigma = 0.01$ the wells are separated by a small barrier, as shown in figure 7($b$). At $HMt_f/\sigma = 0$ (figure 7($c$)) they are equally deep and symmetrically placed about $\theta = 0$.

Reversal of the field causes the $\theta = 3\pi/2$ well to deepen and the $\theta = \pi/2$ well to become shallow. At a large negative field, the $\pi/2$ well becomes unstable and the magnetization

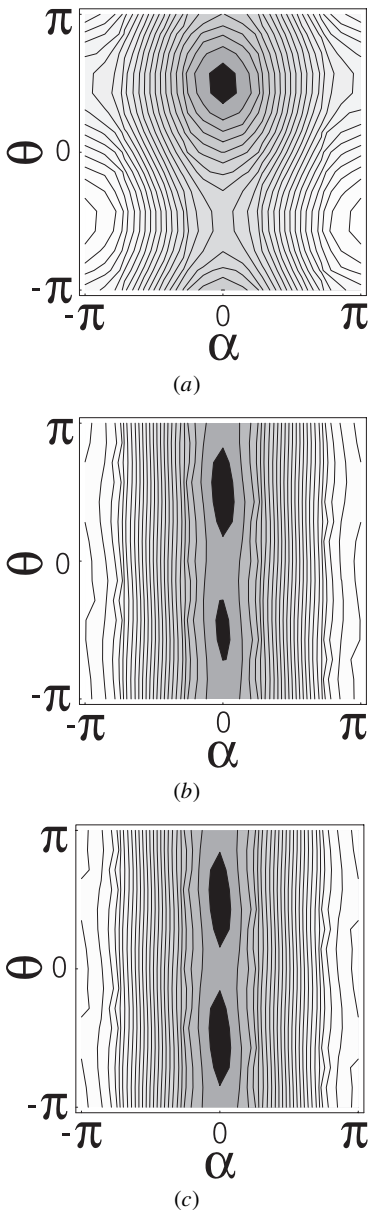


**Figure 7.** Energy contour plots for reversal of the ferromagnet with a compensated interface. The exchange is $J_2 = 0.04$ and the applied field is aligned along $\rho = \pi/2$ with magnitude $HMt_f/\sigma = 0.5$ in ($a$), $HMt_f/\sigma = 0.01$ in ($b$) and $HMt_f/\sigma = 0$ in ($c$). The value of $J_2$ is too small for exchange bias in this example, and only irreversible changes of the magnetization from one well to the other are possible.

moves to the $3\pi/2$ well. The magnetization remains in the $\theta = 3\pi/2$ well until it becomes unstable at a large positive field as the field is cycled back into the original cooling direction. The hysteresis is symmetrical about $H = 0$ in this case and there is no exchange bias.

The corresponding hysteresis curve is shown in figure 8 where the magnetization as a function of field is calculated by minimizing the energy in equation (13). The value of $J_2$ used in this example is not large enough to support a biased magnetization curve. An interesting point is that hysteresis appears even though there is no anisotropy in the ferromagnet. The magnitude of the hysteresis depends on the magnitude of $J_2$.

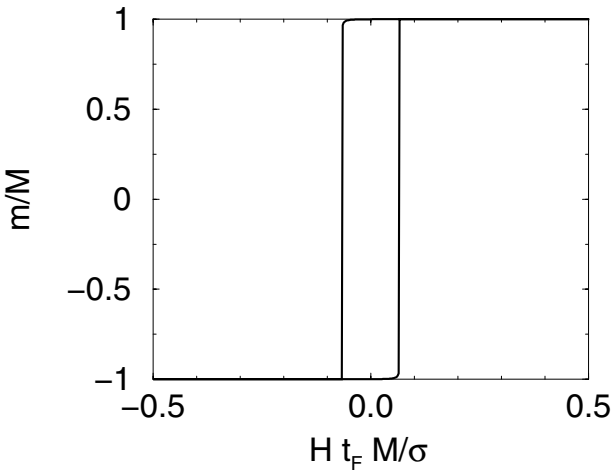


**Figure 8.** Hysteresis for exchange bias with a compensated interface in the partial wall model. The initial potential well becomes unstable and the magnetization shifts to another well at $HMt_f/\sigma = \pm 0.06$. The result is that the ferromagnet follows paths in different quadrants of $\theta$. The hysteresis loop is symmetrical about $H = 0$ so that no bias appears.

If a value for $J_2$ greater than the wall energy is used, numerical micromagnetic models show that a partial wall type of bias can exist (Koon 1997, Kim *et al* 1999). The results obtained from equation (13) in this limit are in qualitative agreement with micromagnetic results, and insight can be gained by examining the energy landscape.

An example of the energy contours with $J_2 = 9$ is shown in figure 9. The most striking feature is a skewing of the valleys so that a path appears for the ferromagnet between $\theta = \pi/2$ and $\theta = 3\pi/2$ that never crosses a barrier. This can be seen by comparing figures 9($a$) and ($b$) where the field is $HMt_f/\sigma = 2$ and $-2$, respectively. If the magnetization begins at saturation in the minimum at $\theta = \pi/2$ (as in figure 9($a$)) then it will remain in the valley containing the minimum as the field is reduced to zero. The minimum shifts, but does not move into the $\theta < 0$ region until $HMt_f/\sigma = -2$. As the field is made more negative, the minimum slowly approaches $\theta = 3\pi/2$. The antiferromagnet is considerably twisted at this point, with a large value of $\alpha$ due to the large $J_2$. The process is reversible if the field is reduced to zero and increased again into the positive direction. The result is a biased magnetization curve without hysteresis, as for the uncompensated example of figure 3.

The reversible bias exists because there is a barrier between wells in two different valleys. The barrier decreases in height as the field is made more negative. If the magnetization crosses this barrier, reversal of the magnetization becomes irreversible and hysteresis appears without exchange bias.

### 3.2. Natural angle and mixed interfaces

There are two important aspects to the mixed interface case. The first is that all of the above considerations regarding stability apply. Irreversible processes are unavoidable for values of exchange less than the wall energy and hysteretic behaviour appears. The second aspect is that although hysteresis appears, the loops may be asymmetric, shifted,

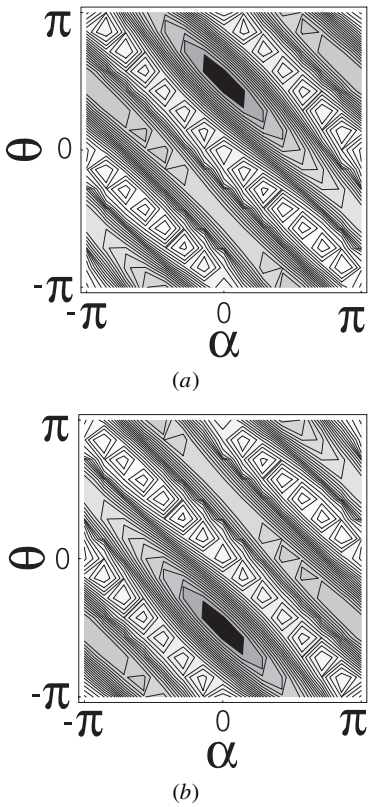


**Figure 9.** Energy contour plots for reversal of a ferromagnet with a compensated interface. Here $J_2 = 3\sigma/2$ and the applied field is again aligned along $\theta = \pi/2$. The applied field magnitude is $HMt_f/\sigma = 2$ in $(a)$ and $HMt_f/\sigma = -2$ in $(b)$. The value of $J_2$ skews the energy valleys in such a way as to provide a path for the ferromagnet that never crosses a barrier. This allows exchange bias to appear as a reversible magnetization process.

or both. The reason is that the magnetization returns through a different quadrant of $\theta$ than it went through in the forward path, and these paths may involve different effective fields because of coupling to both sublattices of the antiferromagnet.

Examples of different forward and return paths are shown by the magnetization loops in figure 10. These loops are calculated with $J_1 = 0.2$ and $J_2 = 0.16$ for different orientations of the applied field. The hysteresis loops are asymmetric about their midpoints and shifted for field orientations between $\rho = 0$ and $\rho = \pi/2$.

The reason for the asymmetry can be understood by comparing the energy landscape for the forward and reverse magnetization paths. Energy contours for an asymmetric case of figure 10 are shown in figure 11 with $\rho = \pi/6$. The field has magnitude $HMt_f/\sigma = +0.5$ in figure 11$(a)$, $HMt_f/\sigma = 0$ in figure 11$(b)$ and $HMt_f/\sigma = -0.5$ in figure 11$(c)$. The key feature is that $J_2$ skews the energy surface so that each well passes through a different set of $\alpha$ values as the field is changed. Because $\alpha$ measures the magnitude of the twist of the partial wall in the antiferromagnet, it also measures the effective field acting on the ferromagnet. Because the forward and reverse paths of the hysteresis curve take the ferromagnet through different sets of effective fields, the shape of the loop in the forward direction can be very different from the shape of the loop in the reverse

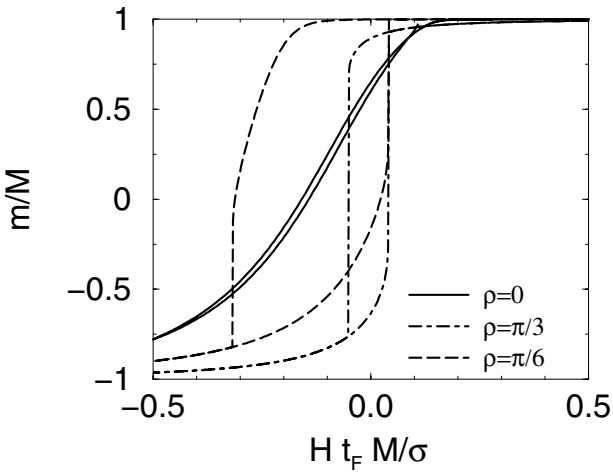


**Figure 10.** Hysteresis loops for a mixed interface with different orientations of the applied field. The exchange parameters are $J_1 = 0.2$ and $J_2 = 0.16$. The angle of the applied field is $\rho$. The loops are asymmetric for most angles.

direction. The result is an asymmetric hysteresis that reflects the different internal effective fields involved when taking the magnetization through the forward and reverse directions.

It is interesting to note that the appearance of asymmetry in hysteresis is sometimes attributed to domain wall pinning and de-pinning along different points on the hysteresis loop (Goodman *et al* 2000). The above explanation is consistent with this view in that it describes de-pinning of partial walls formed in the direction normal to the interface.

The appearance of asymmetric hysteresis can be characterized by the definition of a 'natural' angle, $\theta_{nat}$. This angle specifies the equilibrium orientation of the ferromagnet in zero applied field (Camley *et al* 1999) and will be further discussed below in relation to rough interfaces.

### 3.3. Instability to out-of-plane fluctuations

As illustrated above, exchange bias and coercivity are sensitive to existence conditions for partial wall formation near the interface. The treatment so far has considered only rotations of the ferromagnet and antiferromagnet in a common plane, implicitly assumed to be a plane parallel to the interface. A more general model allows the extra degrees of freedom for the magnetizations in each layer to rotate in separate planes. This is very difficult to treat analytically, and numerical methods are necessary.

Because the film geometry involves large shape anisotropies arising from demagnetizing fields in the ferromagnet, the assumption of in-plane rotation is reasonable for soft ferromagnets. It is then possible to propose, as done by Stiles and McMichael (1999a), a particular type of out-of-plane rotation for magnetization processes in the antiferromagnet. The assumption is that, at least for granular structures, both sublattices of the antiferromagnet can be present at the interface and twists in the antiferromagnet can exist due to canting between the sublattice magnetizations. The idea is that the twist can be reduced or released through a 180° rotation through a plane normal to the interface. This process takes the

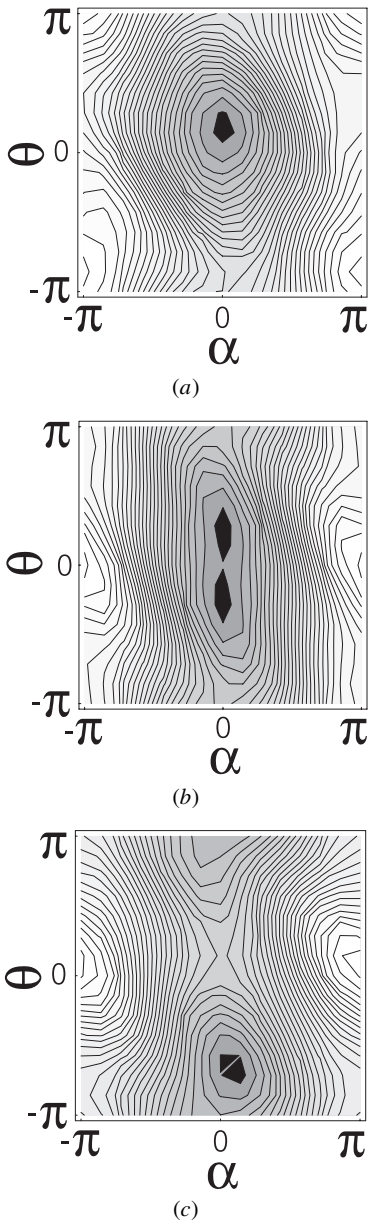


**Figure 11.** Energy surface contour plots for a mixed interface. The applied field is along the $\rho = \pi/6$ direction and $J_1 = 0.2$ and $J_2 = 0.16$ as in figure 10. The energy surface for $HMt_f/\sigma = +0.5$ is shown in ($a$), for $HMt_f/\sigma = 0$ in ($b$), and for $HMt_f/\sigma = -0.5$ in ($c$). Note how different the energy contours are for $\pm H$, corresponding to different magnitudes of effective fields acting on the ferromagnet for forward and reverse magnetization processes.

antiferromagnet moments out of the film plane during this rotation. A sketch of this process is shown in figure 12.

This picture is consistent with numerical simulations on spin lattices for perfectly compensated interfaces (Schulthess and Butler 1998, Kim *et al* 1999, Camley *et al* 1999, Stamps 2000). In these studies, precession of the spins out-of-plane is found to de-pin the partial wall and thereby remove the bias shift in cases where the interface is fully compensated. The energy associated with the out-of-plane rotation depends on the existence of any easy plane anisotropies. An easy plane anisotropy, leading to a preferential planar orientation of the antiferromagnet spins, can serve to stabilize the partial wall

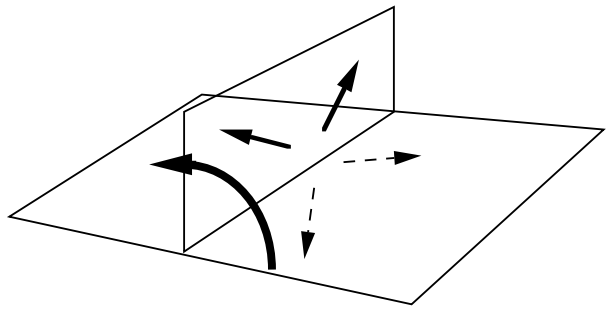

**Figure 12.** Out-of-plane rotation of antiferromagnet moments as an irreversible process. An event is described as the reversal of the moment coupling the antiferromagnet to a ferromagnet. The reversal is accomplished by an out-of-plane rotation, shown here for a compensated interface (Stiles and McMichael 1999b).

in the antiferromagnet against out-of-plane precession. Note that while it is convenient to refer to planes parallel to the interface, in general the same considerations apply to any plane favoured by the antiferromagnet moments.

The above considerations can be quantified by adding a term representing the cost in energy of rotating antiferromagnet moments through an angle $\psi$ specifying an out-of-plane rotation. This term can be estimated by supposing that only moments within a domain wall length $\Delta$ of the interface are involved (Stamps 2000). Allowing for an easy plane anisotropy of magnitude $K_0$, the energy represents a barrier $E_B$:

$$E_B = \Delta K_0 \sin^2 \psi. \tag{15}$$

Inclusion of this energy into equation (13) makes it possible to examine the stability of the exchange bias to fluctuations out of the film plane. Inserting the expression for $E_B$ into equation (13) and allowing for the extra $\psi$ degree of freedom for $\boldsymbol{a}$, stability can be examined by calculating $\frac{\partial^2 E}{\partial \psi^2}$. If the interface is fully compensated such that $J_1 = 0$, a partial wall allowing reversible exchange bias is stable only if

$$\Delta K_0 > J_2. \tag{16}$$

This result assumes that all moments a distance $\Delta$ into the antiferromagnet participate equally. A less restrictive approach is to examine the stability using a numerical simulation for an array of classical spin vectors representing the magnetic moments. Details of the approach taken for this problem are discussed elsewhere (Kim *et al* 1999, Wee and Stamps 2001), but the essentials are as follows.

Vectors $\boldsymbol{S}_i$ are used to represent local magnetic moments and are associated with lattice sites $i$ in a three-dimensional array. The lattice structure is taken as simple cubic with nearest-neighbour exchange $J_{i,j}$ and local site uniaxial anisotropies $K_i$. The ferromagnet layers have a positive $J_{i,j} = J_f$, and the antiferromagnet layers have negative $J_{i,j} = J_{AF}$. The anisotropy is non-zero only in the antiferromagnet. The exchange between moments at the interface is $J_{i,j} = J_I$.

Equilibrium configurations are found by numerically integrating torque equations using a relaxation method. The idea is to find zero torque configurations by numerically integrating the Landau–Lifshitz equations of motion for each spin. Dissipation is included as a damping term that

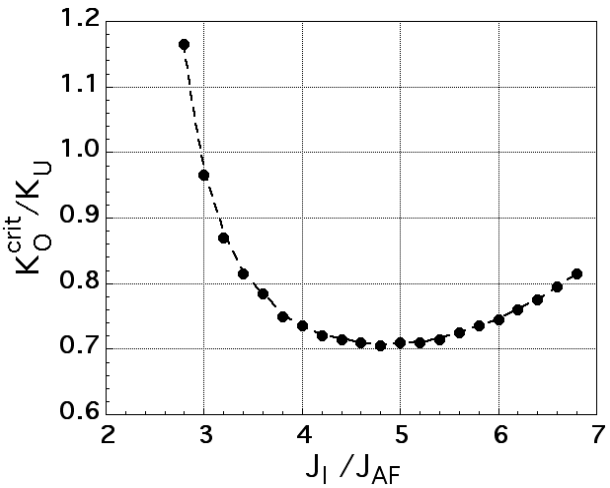


**Figure 13.** Region of stability for exchange bias at a compensated interface. The region above the curve indicates values of $K$ and $J_I$ for which exchange bias is stable for applied fields in the range $-\sigma < HM < \sigma$. Points below this curve do not produce reversible exchange bias (Kim *et al* 1999).

preserves the magnitude of the vectors. After sufficient time, each spin relaxes into an equilibrium orientation where the torques vanish. This method is particularly useful for this problem because it avoids unstable equilibrium configurations that often create problems with other energy minimization techniques.

The Landau–Lifshitz equations of motion for each $\boldsymbol{S}_i$ in the array are

$$\frac{\mathrm{d}}{\mathrm{d}t}\boldsymbol{S}_i = -\gamma \boldsymbol{S}_i \times \nabla_{\boldsymbol{S}_i}\mathcal{H} + \lambda \boldsymbol{S}_i \times \boldsymbol{S}_i \times \nabla_{\boldsymbol{S}_i}\mathcal{H} \qquad (17)$$

where the local effective field is calculated from

$$\mathcal{H} = \sum_{i,j}^{N} J_{i,j}\boldsymbol{S}_i \cdot \boldsymbol{S}_j + \sum_{i}^{N}\left[-g\mu_{\mathrm{B}}\boldsymbol{H}\cdot\boldsymbol{S}_i + K_i\left(\boldsymbol{S}_i \cdot \hat{\boldsymbol{n}}_{\mathrm{af}}\right)^2\right]. \qquad (18)$$

In order to identify coercive mechanisms associated with the antiferromagnet, anisotropy is not included in the ferromagnet. The antiferromagnet anisotropy is uniaxial with the easy axis in the $\boldsymbol{n}_{\mathrm{af}}$ direction. Several numerical integrations were compared, and a fifth-order predictor corrector method appeared to be one of the more stable and efficient for this problem.

This numerical model was used to generate the phase diagram in figure 13. The array consisted of a $4 \times 4 \times 30$ block of vector spins representing ten ferromagnet layers exchange coupled to twenty antiferromagnet layers. The exchange coupling the two layers is $J_{\mathrm{I}}$. Regions above the curve correspond to values of $J_{\mathrm{I}}$ and $K$ for which exchange bias is stable for applied fields in the range $-\sigma < HM < \sigma$. The region below the curve are values that do not produce exchange bias in this field range.

### 3.4. Exchange bias at rough interfaces

Certain crystallographic orientations can produce flat, mixed interfaces but, in general, mixed interfaces may be due to geometric roughness. There have been several experiments

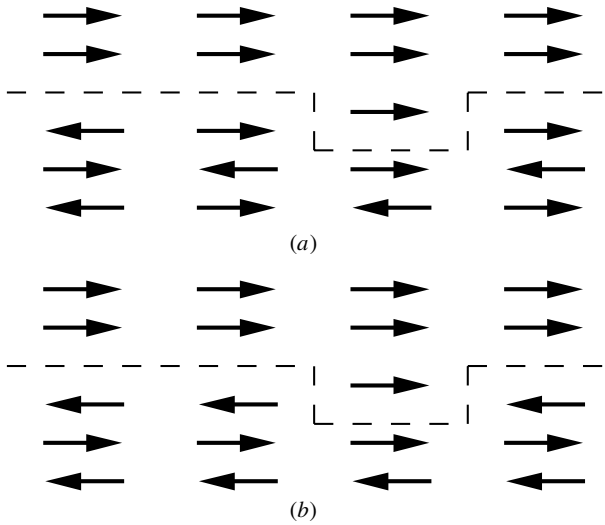


**Figure 14.** Schematic diagram of geometric roughness at interfaces. Roughness produced by line defects is sketched for (*a*) a compensated interface and (*b*) an uncompensated interface (Kim *et al* 2000).

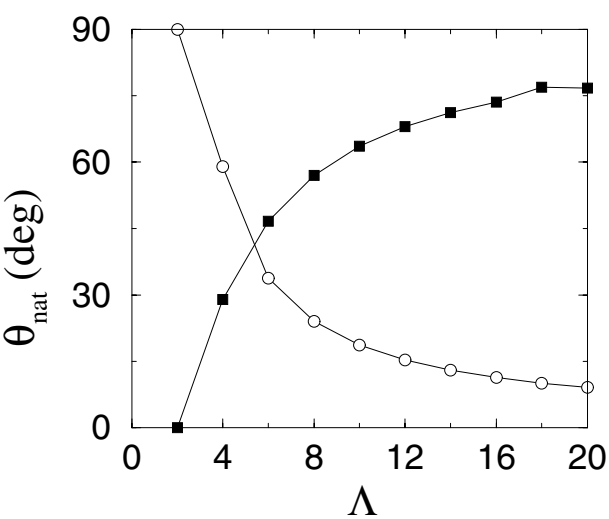


**Figure 15.** Modification of the natural angle with interface line defects. The natural angle for compensated (solid squares) and uncompensated (open circles) interfaces is shown as a function of line spacing. The natural angle can be varied over a 90° range in each case (Kim *et al* 2000).

that examine aspects of the interface and film quality (Uyama *et al* 1997, Lederman *et al* 1997, Escorcia-Aparicio 1998, Nogués *et al* 1999, Sort *et al* 1999, Schulthess and Butler 1999, Chopra *et al* 2000, Leighton *et al* 2000).

For numerical simulation, a structured interface along one direction was examined. An example is sketched in figure 14 for lines of ferromagnet moments penetrating into the antiferromagnet at compensated and uncompensated interfaces. Results from numerical simulations of interfaces with line defects display features similar to those described in the previous section for mixed interfaces. In particular, there is a natural angle for the zero field orientation of the ferromagnet. The magnitude of the angle depends on the density of lines, and can be varied over a 90° range.

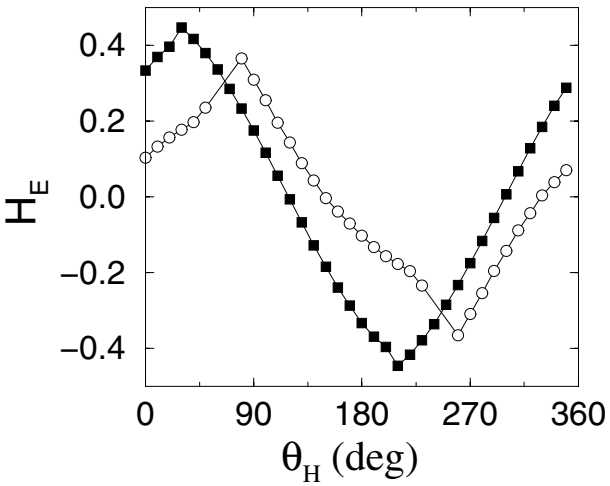


**Figure 16.** Exchange bias with line defects as a function of applied field orientation. The line spacing is $\Lambda = 4$. The solid squares represent line defects at a compensated interface, and the open circles represent line defects at an uncompensated interface (Kim *et al* 2000).

This dependence is shown in figure 15 where the natural angle $\theta_{\text{nat}}$ is shown as a function of spacing $\Lambda$ between interface line defects. Results for compensated interfaces are shown by the solid squares, and for uncompensated interfaces by the open circles. The extreme values at $\Lambda = 2$ correspond to the situation of an initially fully compensated interface made uncompensated by alternating lines of defects across the interface. Similarly, the converse of an initially uncompensated interface made compensated is also possible. A change in the natural angle appears as a change in the magnitude for different orientation angles, ($\theta_{\text{H}}$ in this figure) of the applied field. An example is shown in figure 16, calculated using the numerical spin array model with $J_{\text{I}} = 10J$. The solid squares represent a compensated interface with line defects spaced with period $\Lambda = 4$. The open circles represent an uncompensated interface with line defects spaced with the same period.

The main effect is a shift of the bias field maximum from the perfect interface values of 90° for the compensated interface, and 0° for the uncompensated interface. The shift is the magnitude of the natural angle. Note the discontinuities near the extrema of the bias curves. These signal the instability of the ferromagnet configuration and the subsequent reconfiguration into different energy minima. These results appear to be consistent with experimental data reported by Nogués *et al* (1999).

This behaviour can be conveniently characterized through the idea of natural angle introduced earlier. The asymmetry in twist angle is depicted in figure 17 where the two paths taken by the ferromagnet magnetization are indicated in terms of the antiferromagnet twist and natural angle. Clockwise rotation of the ferromagnet magnetization in the initial field cooled potential well is shown by figure 17($a$) for the natural angle, $\theta_{\text{nat}}$, greater than the angle of the applied field. This creates a twist in the antiferromagnet of magnitude $\phi_1$ as shown in figure 17($b$). Counterclockwise rotation with $\theta_{\text{nat}}$ less than the angle of the applied field, indicated in figure 17($c$), is associated with being in the other potential well. This has a different associated natural angle, and creates a different magnitude twist $\phi_2$, as shown in figure 17($d$).

### 3.5. Random defects: bias enhancement and coercivity

The importance of domain structure and dynamics on exchange bias was recognized in the earliest experiments (Meiklejohn 1962). Malozemoff (1987) made quantitative estimates of reduced exchange bias fields based on a domain wall pinning model. Recent experiments using ion-irradiation and non-magnetic impurity implantation techniques have provided useful additional experimental input on the problem (Mewes *et al* 2000, Miltényi *et al* 2000). A particularly interesting finding has been the observation of enhancements of the bias for low numbers of defects. One argument is that the initial introduction of defects serves to free unsaturated domains (Miltényi *et al* 2000).

The numerical approach described above was used to examine effects of local changes in anisotropy and exchange on the magnetic hysteresis of exchange bias structures (Kim and Stamps 2001). A summary of results is shown in figure 18 for an uncompensated interface. The normalized bias field was calculated with defects placed in a particular layer $L$ of the antiferromagnet. In figure 18($a$), the exchange integral $J_{i,j}$ is reduced to zero at random sites within a layer of spins in the antiferromagnet. Each layer is indexed by an integer $L$ where the interfacial layer is $L = 0$ and the bottom layer is $L = 14$. The layer defect density, $n(L)$, is defined by the fraction of the unit cell that is occupied by imperfections.

The bias field decreases to zero quickly with $n$ for defects located at or near the interface. Defects in layers deeper in the antiferromagnet cause the bias field to decrease with a different functional dependence on $n$. Defects more than a domain wall length away from the interface have little effect on the bias field. In figure 18($b$), only the anisotropy $K_i$ is changed at random sites within a layer at $L$. The anisotropy at chosen sites is increased by a factor of 10 from the other sites. The effect of increasing the anisotropy is to change the partial domain wall energy in the antiferromagnet and increase the bias field. The largest enhancement of the bias field occurs for imperfections placed directly at the interface. Note that it is possible to obtain an enhancement of the bias field at small defect concentrations by simultaneously reducing exchange near defects and increasing anisotropy. The enhancement is governed primarily by interface exchange and anisotropy.

A similar increase in the bias field is observed for local enhancements of anisotropy for compensated interfaces, but larger defect concentrations result in a complete suppression of exchange-bias. This suppression appears to be linked with the inability to form partial walls in the antiferromagnet. Coercivity is strongly affected with the creation of large, asymmetric hysteresis loops. Defects responsible for changes in coercivity were found to be primarily associated with locations in the antiferromagnet away from the interface. The asymmetry results from the pinning of the antiferromagnet wall formed as the ferromagnet rotates into the reverse field. As the external field is increased in the forward direction, the wall is de-pinned and the ferromagnet aligns with the field.

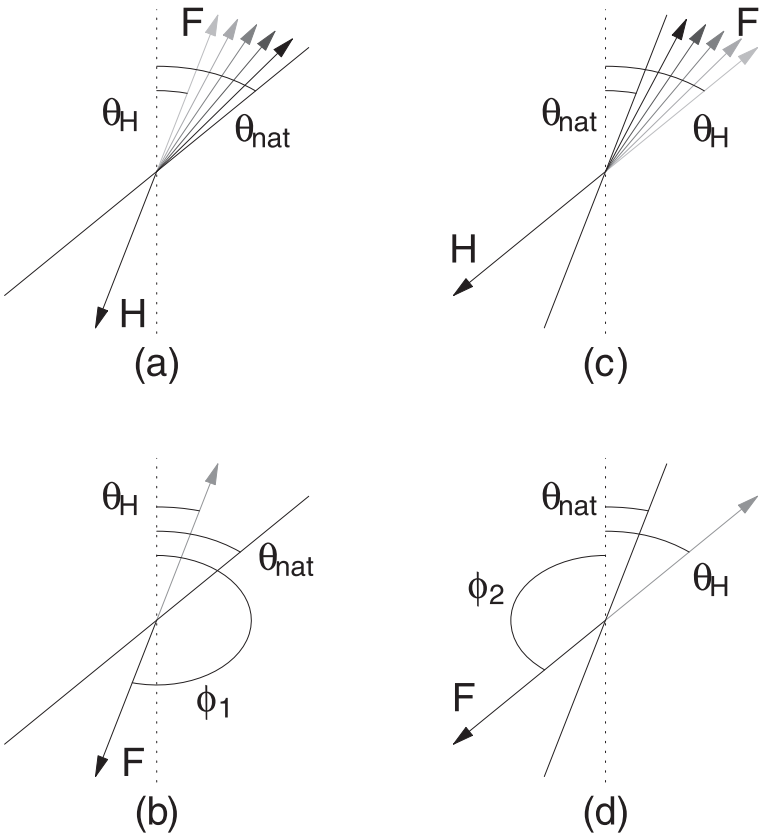


**Figure 17.** Asymmetry of the antiferromagnet twist for a mixed interface. Clockwise rotation of the ferromagnet magnetization with $\theta_{\text{nat}}$ greater than the applied field angle is shown in (*a*) and (*b*). This creates a twist in the antiferromagnet of magnitude $\phi_1$ as shown in (*b*). Counterclockwise rotation for $\theta_{\text{nat}}$ less than the applied field angle is shown in (*c*) and (*d*). The magnitude twist $\phi_2$ is different from $\phi_1$ (Kim *et al* 2000).

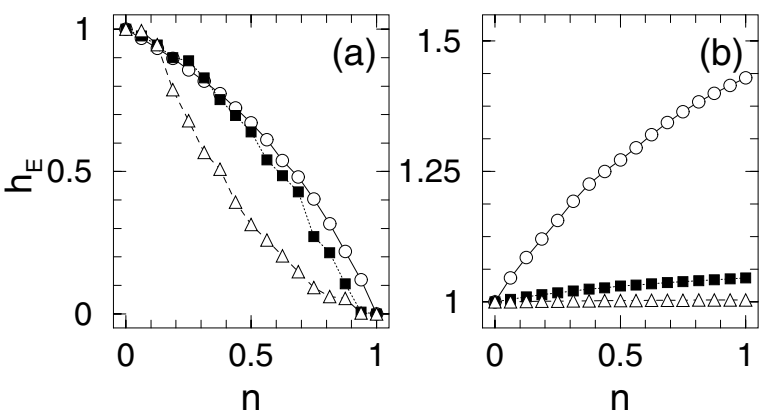


**Figure 18.** The bias field calculated as a function of layer defect concentration $n(L)$, with defects represented as (*a*) reduced $J_{i,j}$ and (*b*) increased $K_i$ for an uncompensated interface. The circles represent $L = 0$, the squares represent $L = 2$, and the triangles represent $L = 4$. Note the competing effects of reduced interface exchange and increased interface anisotropy.

## 4. Theory of exchange bias

The previous two sections contain descriptions of exchange bias and coercivity based on models for partial wall formation and asymmetric hysteresis. With the exception of the numerical simulations, the models are formulated in terms of the energy given in equation (13). The numerical simulations allow explorations of structural dependences in that they are formulated in terms of a spin vector array model given by equation (18).

The purpose of this section is to build a connection between these two approaches. This will be accomplished with a justification of the use of equation (13) by showing that it follows directly from equation (18). As a consequence, it will be seen that the bilinear and biquadratic exchange terms in equation (13) are related to and determined by the degree of compensation at the interface. It will also be shown that the ratio $J_1/\sqrt{J_2}$ relates directly to the relative fractions of each antiferromagnet sublattice present at the interface.

### 4.1. Transition to a continuum and interface region

The first step in bridging the gap between equations (18) and (13) is to go from a discrete array of lattice spin vectors to a continuous field of magnetizations. This is done in the usual way by replacing the spin vector $\boldsymbol{S}_i$ at a site $i$ by the continuous variable $\boldsymbol{S}(\boldsymbol{x})$. Coupling terms between spins at neighbouring sites are dealt with by assuming that $\boldsymbol{S}(\boldsymbol{x})$ changes slowly over lattice spacing length scales.

The beginning energy is based on the Hamiltonian of equation (18) and is written in a notation that explicitly distinguishes between spins in the ferromagnet and each antiferromagnet sublattice. The respective lattice vectors are identified by unit vectors $\boldsymbol{f}_i$, $\boldsymbol{a}_i$ and $\boldsymbol{b}_i$. The total energy is written as a sum of energies in the ferromagnet, antiferromagnet and at the interface:

$$E = E_{\mathrm{f}} + E_{\mathrm{af}} + E_{\mathrm{inter}}. \tag{19}$$

The energy in the ferromagnet is

$$E_{\mathrm{f}} = \sum_{i\in\mathrm{ferro}} \left[ -\boldsymbol{H}\cdot\boldsymbol{f}_i - \sum_{\langle i,j\rangle} J_{i,j}\boldsymbol{f}_i\cdot\boldsymbol{f}_j - K_i\left(\boldsymbol{f}_i\cdot\hat{\boldsymbol{n}}_{\mathrm{f}}\right)^2 \right] \tag{20}$$

the energy in the antiferromagnet is

$$E_{\mathrm{af}} = \sum_{i\in\mathrm{antiferro}} \left[ -\boldsymbol{H}\cdot(\boldsymbol{a}_i + \boldsymbol{b}_i + \sum_{\langle i,j\rangle} J_{i,j}\boldsymbol{a}_i\cdot\boldsymbol{b}_j - K_i \times \left[\left(\boldsymbol{a}_i\cdot\hat{\boldsymbol{n}}_{\mathrm{af}}\right)^2 + \left(\boldsymbol{b}_i\cdot\hat{\boldsymbol{n}}_{\mathrm{af}}\right)^2\right]\right] \tag{21}$$

and the exchange coupling energy across the interface is

$$E_{\mathrm{inter}} = \sum_{i,j\in\mathrm{interface}} J_{\mathrm{a}}\boldsymbol{f}_i\cdot\boldsymbol{a}_j - \sum_{\langle i,j\rangle} J_{\mathrm{b}}\boldsymbol{f}_i\cdot\boldsymbol{b}_j. \tag{22}$$

At this point it is convenient to transform the antiferromagnet spin vectors into a new representation that will be useful for discussing the case of canted interface spins. The representation is in terms of longitudinal and transverse vectors $\boldsymbol{l}_i$ and $\boldsymbol{t}_i$ defined as

$$\boldsymbol{l}_i = \boldsymbol{a}_i + \boldsymbol{b}_i \tag{23}$$

$$\boldsymbol{t}_i = \boldsymbol{a}_i - \boldsymbol{b}_i. \tag{24}$$

The next step is to rewrite the energies in terms of spin vector variables that are continuous functions of position. These are $\boldsymbol{f}(\boldsymbol{x})$ for the ferromagnet, $\boldsymbol{l}(\boldsymbol{x})$ and $\boldsymbol{t}(\boldsymbol{x})$ for the antiferromagnet. The exchange energy terms are constructed by expanding the spin vector fields about neighbouring lattice sites. For example, if the vector pointing from the site at $i$ to the site at $j$ is $\boldsymbol{\delta}$, then

$$\boldsymbol{f}(\boldsymbol{x}+\boldsymbol{\delta}) \approx \boldsymbol{f}(\boldsymbol{x}) + \delta\cdot\nabla\boldsymbol{f}(\boldsymbol{x}) + \tfrac{1}{2}(\delta\cdot\nabla)^2\boldsymbol{f}(\boldsymbol{x}). \tag{25}$$

This procedure is followed for each of the magnetization fields. Away from the surfaces and interfaces, the terms linear in $\delta$ vanish in the exchange energy sums, leaving only the terms quadratic in $\delta$. At the outer surfaces, this is not the case, and there are associated boundary conditions that can act to pin dynamic fluctuations. These dynamic pinning equations are automatically satisfied at the free surfaces by solutions to the equilibrium problem.

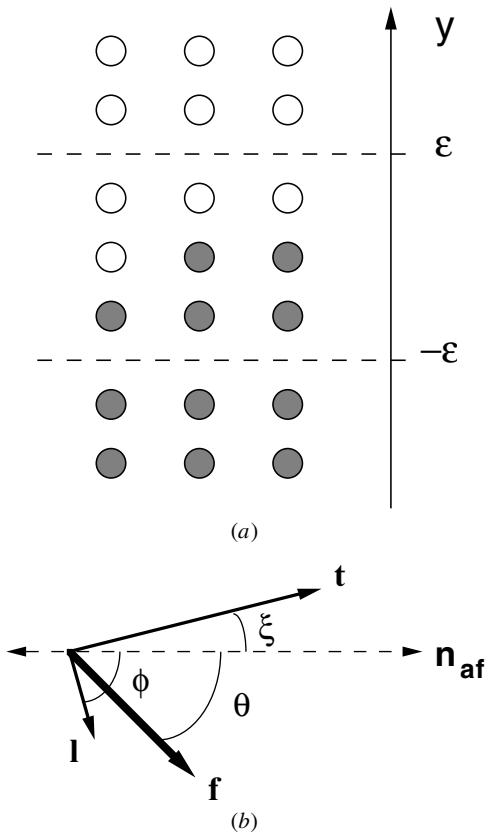


**Figure 19.** Geometry. The interface region is sketched in ($a$). The antiferromagnet is in the $y < \epsilon$ half space, and the ferromagnet is in the $y > \epsilon$ half space. The interface region contains magnetic moments from each material and the boundaries are defined to intercept only exchange couplings between like moments. In ($b$), the angles $\theta$, $\phi$, and $\xi$ are defined, specifying the transformed magnetizations. The angles are functions of position, $y$.

The boundary conditions at the interface between the ferromagnet and antiferromagnet may be imperfect and difficult to treat in a manner useful for further analytic calculations. For this reason, an interface region is defined between the ferromagnet and the antiferromagnet. The geometry of this region is shown in figure 19. The interface region extends between $y = +\epsilon$ and $y = -\epsilon$, and the boundaries are defined to lie in regions where the material is homogeneous. The boundary at $y = -\epsilon$ intercepts only exchange couplings between antiferromagnet moments, and the boundary at $y = \epsilon$ intercepts only exchange couplings between ferromagnet moments. The advantage of this definition is that in going from discrete sums to integrals, the exchange energy terms in $E_{\mathrm{f}}$ and $E_{\mathrm{af}}$ will not lead to additional boundary conditions due to discontinuities in the magnetization fields at the boundaries with the interface region. Formulated this way, an average over the interface region can be made such that roughness and imperfection effects can be treated with the definition of average exchange coupling parameters.

For simplicity, variations in the magnetizations parallel to the interface plane are not considered, so that $\boldsymbol{f}$, $\boldsymbol{l}$ and $\boldsymbol{t}$ depend only on $y$. The energies per area in the ferromagnet

and antiferromagnet are

$$\mathcal{E}_{\rm f} = \int_{\epsilon}^{\infty} \left[ -\boldsymbol{H}\cdot\boldsymbol{f} - K_{\rm f}\,(\boldsymbol{f}\cdot\boldsymbol{n}_{\rm f})^2 - \boldsymbol{f}\cdot D_{\rm f}\frac{\partial^2}{\partial y^2}\boldsymbol{f}\right] {\rm d}y \tag{26}$$

$$\mathcal{E}_{\rm af} = \int_{-\infty}^{-\epsilon} \Bigg[ -\boldsymbol{H}\cdot\boldsymbol{l} - K_{\rm af}\left[(\boldsymbol{l}\cdot\boldsymbol{n}_{\rm af})^2 + (\boldsymbol{t}\cdot\boldsymbol{n}_{\rm af})^2\right] + D_{\rm af}\left(\boldsymbol{t}\cdot\frac{\partial^2}{\partial y^2}\boldsymbol{t} - \boldsymbol{l}\cdot\frac{\partial^2}{\partial y^2}\boldsymbol{l}\right)\Bigg] {\rm d}y. \tag{27}$$

Exchange stiffness constants have been defined as $D_{\rm f} = z_{\rm f} J_{\rm f}\delta^2/2$ and $D_{\rm af} = z_{\rm af} J_{\rm af}\delta^2/2$ to include all geometrical information, such as coordination number and lattice spacing.

An exchange energy in the interface region is now constructed. The thickness of the region is $2\epsilon$ and is assumed to be small. The interface is assumed to be mixed on length scales small enough such that average exchange coupling integrals $J_{\rm a}$ and $J_{\rm b}$ can be defined as a measure of the average coupling between the ferromagnet and the two antiferromagnet sublattices. The interface exchange energy per area is then written as

$$\mathcal{E}_{\rm inter} = 2\epsilon\left[J_{+}\boldsymbol{f}\cdot\boldsymbol{l} + J_{-}\boldsymbol{f}\cdot\boldsymbol{t}\right] \tag{28}$$

where

$$J_{\pm} = J_{\rm a} \pm J_{\rm b}. \tag{29}$$

The $J_{\pm}$ will turn out to be related to the $J_1$ and $J_2$ parameters introduced in section 2.

### 4.2. Energy minimization and boundary conditions

The total energy per area, $\mathcal{E} = \mathcal{E}_{\rm f} + \mathcal{E}_{\rm af} + \mathcal{E}_{\rm inter}$, is to be minimized by considering variations of the orientations of $\boldsymbol{f}$, $\boldsymbol{l}$ and $\boldsymbol{t}$. There are also constraints to be considered, namely that $|\boldsymbol{f}| = 1$ and $|\boldsymbol{a}| = |\boldsymbol{b}| = 1$. The latter implies that $\boldsymbol{l}$ and $\boldsymbol{t}$ are constrained by the relation

$$l^2 + t^2 = 2. \tag{30}$$

The constraints can be conveniently imposed by using an angular representation for the magnetizations. In addition to $\theta$ defined in figure 5, the angle $\phi$ is defined for the $\boldsymbol{l}$ and $\boldsymbol{t}$ vectors. This is referenced to the same direction as $\theta$ and is illustrated in figure 19($b$). It is also necessary to define an angle to specify the direction of $\boldsymbol{l}$ relative to the sublattice moments. This is done with the angle $\xi$ also shown in figure 19($b$). The magnitudes of the antiferromagnet magnetizations are then $|\boldsymbol{l}| = \sqrt{2}\cos\xi$ and $|\boldsymbol{t}| = \sqrt{2}\sin\xi$, consistent with equation (30). Note that the magnetization angles are functions of $y$.

A simplification can now be made for the case of large antiferromagnet exchange coupling. If $D_{\rm af}$ is large, the sublattice magnetizations remain nearly antiparallel everywhere. This means $|\boldsymbol{l}|$ is small, which suggests expanding $\xi$ about $\pi/2$. Defining $\beta = \pi/2 - \xi$, where $\beta \ll 1$, the total energy per area can be written as

$$\begin{aligned}\mathcal{E} \approx \int_{\phi}^{\infty} &\left[-HM\cos(\theta-\rho) + D_{\rm f}\theta_y^2 - K_{\rm f}\cos^2\theta\right] {\rm d}y \\ &+ \int_{-\infty}^{\phi} \Big[ -\sqrt{2}HM\cos(\phi-\rho)\beta \\ &+2D_{\rm af}\left(1-2\beta^2\right)\left(\beta_y^2 - \phi_y^2\right) \\ &-2K_{\rm af}\left(\beta^2\cos^2\phi + \left(1-\beta^2\right)\sin^2\phi\right)\Big] {\rm d}y \\ &+\sqrt{2}\epsilon\Big[J_{+}\beta_0\cos(\theta_0-\phi_0) - J_{-}\left(1-\tfrac{1}{2}\beta_0^2\right) \\ &\times\sin(\theta_0-\phi_0)\Big].\end{aligned} \tag{31}$$

Because the angles are assumed to be constant over the interface region, $\epsilon$ is set to zero as a limit in the integrals and the interface energy contributions are evaluated at $y = 0$. The subscripted angles $\theta_0$, $\beta_0$ and $\phi_0$ denote evaluation at $y = 0$. Note that $\beta$ is the magnitude of the interface antiferromagnet moment, and that the interlayer exchange $J_{+}$ term is linear in $\beta$. This term couples the ferromagnet to the net interface moment and, in the case of full compensation where $J_{-} = 0$, is the only interlayer exchange coupling.

The extrema of the energy are found by varying $\mathcal{E}$ with respect to each angle:

$$\frac{\delta\mathcal{E}}{\delta\theta} = \frac{\delta\mathcal{E}}{\delta\beta} = \frac{\delta\mathcal{E}}{\delta\phi} = 0. \tag{32}$$

These relations result in three differential equations with associated boundary conditions. The boundary conditions at $y = \pm\infty$ are satisfied by requiring the first derivatives of each angle ($\theta_y$, $\beta_y$, $\phi_y$) to vanish at infinity. The boundary conditions at $\pm\epsilon$ involve terms obtained from the variations of $\mathcal{E}_{\rm inter}$.

Using the notation $x_{yy} = \frac{\partial^2 x}{\partial y^2}$, an equation for the antiferromagnet determined by varying $\phi$ is

$$\begin{aligned}&4D_{\rm af}\left(2\beta^2-1\right)\phi_{yy} + 16D_{\rm af}\beta\beta_y - \sqrt{2}\beta HM\sin(\phi-\rho) \\ &\quad -2K_{\rm af}\left(1-2\beta^2\right)\sin(2\phi) = 0.\end{aligned} \tag{33}$$

The associated interface boundary condition is

$$\begin{aligned}&4D_{\rm af}\left(2\beta_0^2-1\right)\phi_y(0) + \sqrt{2}\epsilon\big[J_{+}\beta_0\sin(\theta_0-\phi_0) \\ &\quad +J_{-}\left(1-\tfrac{1}{2}\beta^2\right)\cos\left(\theta_0-\phi_0\right)\big] = 0.\end{aligned} \tag{34}$$

Similarly, the equation for the longitudinal antiferromagnet component $\beta$ is

$$\begin{aligned}&4D_{\rm af}\left(2\beta^2-1\right)\beta_{yy} + 8D_{\rm af}\beta\beta_y^2 - \sqrt{2}HM\cos(\phi-\rho) \\ &\quad -4K_{\rm af}\beta\cos(2\phi) = 0\end{aligned} \tag{35}$$

with the interface boundary condition

$$\begin{aligned}&4D_{\rm af}\left(2\beta_0^2-1\right)\beta_y(0) - \sqrt{2}\epsilon \\ &\quad\times\left[J_{+}\cos(\theta_0-\phi_0) + J_{-}\beta_0\sin(\theta_0-\phi_0)\right] = 0.\end{aligned} \tag{36}$$

For the moment, it is sufficient to consider a thin ferromagnet film and neglect any deformation of the ferromagnet order. With the assumption that $\theta$ is independent of film thickness, the energy in the ferromagnet is $\mathcal{E}_{\rm f} = -HMt_{\rm f}\cos(\theta-\rho)$. The minimization condition for $\theta$ requires

$$\begin{aligned}&HMt_{\rm f}\sin(\theta_0-\rho) - 2\sqrt{2}\epsilon \\ &\quad\times\left[J_{+}\beta_0\sin(\theta_0-\phi_0) + J_{-}\cos(\theta_0-\phi_0)\right] = \phi.\end{aligned} \tag{37}$$

This last equation is the boundary condition on the ferromagnet. Note that the interlayer exchange part of the boundary conditions for $\theta$ and $\phi$ are the same to first order in $\beta$. For simplicity, anisotropy in the ferromagnet is also neglected.

### 4.3. The interface exchange energy

An expression for the system energy of the form proposed in equation (13) is now constructed. Assumptions are that canting of the antiferromagnet at the interface is small and that there is no significant twist in the ferromagnet.

The assumption that the canting in the antiferromagnet is small means that $\beta$ and $\beta_y$ are small. This allows equation (35) to be linearized. The solutions of the linearized equation are exponential for certain values of $\phi_0$:

$$\beta = C_{\pm} \exp(\pm \Delta y) \tag{38}$$

where

$$\Delta = \sqrt{\frac{K_{\mathrm{af}}}{D_{\mathrm{af}}} \cos(2\phi_0)}. \tag{39}$$

The negative solution diverges as $y \to -\infty$, so the positive solution is chosen. The solution describes an antiferromagnet canted at the interface with a net moment of magnitude $\beta_0$. Far from the interface, the sublattices are antiparallel with no canting. This solution only applies for a restricted range of $\phi$. Outside this range, the solution becomes oscillatory and is no longer localized to the interface.

In order for $\phi$ to become large, it is necessary to induce a significant twist into the antiferromagnet. This in turn requires a strong interlayer exchange and a sizable moment $\beta$. The linearized theory discussed above is not valid in this case and additional orders of $\beta$ would need to be kept in equation (35). The observation that $\phi$ is small also allows the approximation

$$\Delta \approx \sqrt{\frac{K_{\mathrm{af}}}{D_{\mathrm{af}}}}. \tag{40}$$

The boundary condition, equation (36), determines $C$:

$$C = -\frac{J_+ \cos(\theta_0 - \phi_0)}{\sigma_\beta + J_- \sin(\theta_0 - \phi_0)}. \tag{41}$$

Here $\sigma_\beta = 4\sqrt{K_{\mathrm{af}} D_{\mathrm{af}}}/\sqrt{2}$. Because the interlayer coupling cannot be large, then $J_-/\sigma_\beta$ can be treated as an expansion parameter. The resulting expression for $\beta_0$ is then substituted into the ferromagnet and antiferromagnet boundary conditions given by equations (37) and (34). Keeping only lowest order $J_-$ terms in $C$, the result for the ferromagnet boundary condition becomes

$$HMt_{\mathrm{f}} \sin(\theta_0 - \rho) - \theta_- \sin(\theta_0 + \alpha_0) - \frac{\theta_+^2}{\sigma_{\mathrm{a}}} \sin(\theta_0 + \alpha_0) \cos(\theta_0 + \alpha_0) = 0. \tag{42}$$

Note that the angle $\phi$ has been written in terms of $\alpha$ and that $\alpha_0$ denotes $\alpha(0)$.

As noted previously, the boundary condition for the antiferromagnet angle $\phi$ contains identical interlayer exchange terms but involves $\phi_y(0)$. It is straightforward to solve equation (33) for $\phi(y)$ and $\phi_y(y)$. Substitution into the boundary condition equation (34) results in

$$\sigma_{\mathrm{a}} \sin\phi_0 - \theta_- \sin(\theta_0 + \alpha_0) - \frac{\theta_+^2}{\sigma_{\mathrm{a}}} \sin(\theta_0 + \alpha_0) \cos(\theta_0 + \alpha_0) = 0. \tag{43}$$

Here $\sigma_{\mathrm{a}} = 8\sqrt{K_{\mathrm{af}} D_{\mathrm{af}}}$ and $\theta_\pm = 2\sqrt{2} \in J_\pm$. This completes the justification of the interlayer energy proposed in equation (13). Both minimization conditions, equations (42) and (43), can be obtained from equation (13) if the following identifications are made:

$$J_1 = 2\sqrt{2} \in (J_{\mathrm{a}} - J_{\mathrm{b}}) \tag{44}$$

$$J_2 = \frac{\left[2\sqrt{2} \in (J_{\mathrm{a}} + J_{\mathrm{b}})\right]^2}{2\sigma_{\mathrm{a}}}. \tag{45}$$

The biquadratic $J_2$ term involves the sum of the two sublattice exchange terms to second order and is present even in the case of completely uncompensated interfaces where either $J_{\mathrm{a}}$ or $J_{\mathrm{b}}$ is zero. However, in the case of full compensation, where $J_{\mathrm{a}} = J_{\mathrm{b}}$, only biquadratic coupling is possible.

As stressed above, the identifications in equation (45) are based on arguments supposing that $\beta$ and $\phi$ are small. This is consistent with interlayer exchange coupling that is also relatively weak, at least when compared to the magnitude of the energy of wall formation $\sigma_\beta$. These are physically reasonable assumptions and restrictions, and are sufficiently general to include the case of exchange bias by asymmetric loop formation described in section 3. The only cases in which the energy in equation (13) has not been shown to be a good approximation are ones in which $J_+$ is comparable to or greater than $\sigma_\beta$.

Finally, it is interesting to note that measurement of the ratio $J_1/\sqrt{J_2}$ is proportional to the degree of compensation $f$:

$$f = \frac{J_{\mathrm{a}} - J_{\mathrm{b}}}{J_{\mathrm{a}} + J_{\mathrm{b}}}. \tag{46}$$

### 4.4. Partial wall in the ferromagnet

As suggested by Kiwi *et al* (1999b), partial wall formation in the ferromagnet can also support exchange bias at a compensated interface. This can also be obtained from the above theory in limiting cases of thick and thin films.

The general minimization condition on $\theta$ for the ferromagnet is

$$2D_{\mathrm{f}}\theta_{yy} - HM \sin(\theta - \rho) - K_{\mathrm{f}} \sin(2\theta) = 0 \tag{47}$$

with the associated interface boundary condition

$$2D_{\mathrm{f}}\theta_y(0) + 2\sqrt{2}\epsilon \left[J_+ \beta_0 \sin(\theta_0 - \phi_0) + J_- \cos(\theta_0 - \phi_0)\right] = 0. \tag{48}$$

Neglecting $K_{\mathrm{f}}$, solutions for $\theta(y)$ and $\theta_y(y)$ can be derived and used to calculate an energy $\mathcal{E}_{\mathrm{f}}$. In the limit of a very thick ferromagnet, such that $\theta(t_{\mathrm{f}}) = \rho$, this energy has the form

$$\mathcal{E}_{\mathrm{f}} = 2HMt_{\mathrm{f}} + \tfrac{1}{2}\sqrt{HMD_{\mathrm{f}}} \sin\left(\theta_0 - \rho - t_{\mathrm{f}}\sqrt{2HM/D_{\mathrm{f}}}\right). \tag{49}$$

Numerical analysis shows that the ferromagnet partial wall model can produce a reversible exchange bias if $J_2$ is larger than $\sqrt{HMD_{\mathrm{f}}}$ for the entire range of magnetic $H$ fields.

## 5. Exchange bias at finite temperatures

A natural question to ask, when considering stability conditions for magnetic configurations near the interface, is how exchange bias and coercivity are influenced by thermal fluctuations. One way to approach the problem is to use to derive thermally averaged effective fields from equation (18) and to examine how the stability of magnetic configurations change with temperature. This can be accomplished with a mean field approach which provides a useful description for equilibrium averages.

Thermal fluctuations are also important, and cause the exchange bias and coercivity to display time-dependent behaviour in analogy to viscous effects observed for ferromagnets. This idea has been examined by several authors (Néel 1988, Fulcomer and Charap 1972, Stiles and McMichael 1999b, Stamps 2000), and studied experimentally for a number of systems (Schlenker 1968b, Schlenker *et al* 1986, Goodman *et al* 1999, 2000, Geoghegan *et al* 1998). Fluctuations are particularly important in understanding how equilibrium is established because the stability of a given magnetic state depends on the existence of energy barriers separating one configuration from another. Thermal fluctuations can cause irreversible transitions between configurations, and there is always some probability that such an event will occur in a finite time at any temperature $T$.

Results from mean field theory are discussed below, followed by a description of thermal activation processes using Monte Carlo simulations.

### 5.1. Mean field theory and exchange bias

Thermally averaged behaviour of the exchange bias can be calculated using a modified version of the numerical model described in section 3 (Kim *et al* 1999, McGrath and Camley 2000, Wee and Stamps 2001). Thermal averages of the effective fields appearing in the equations of motion, equation (17), are made and used in the calculation of magnetization. Thermally averaged effective fields $\boldsymbol{H}_i$ are calculated from equation (18) using the Brillouin function $B(x)$ in the substitution (Carrico *et al* 1994)

$$S_i^z \rightarrow \langle S_i^z \rangle = S\, B(g\mu_B \boldsymbol{S}_i \cdot \boldsymbol{H}_i / k_B T). \qquad (50)$$

Temperature is $T$ and $k_B$ is Boltzmann's constant. Here $S_i^z$ refers to the component of $\boldsymbol{S}_i$ along the equilibrium direction at site $i$.

Note that the thermal average introduces a self-consistency problem into the calculation of the effective fields at every array site $i$. Determination of the equilibrium direction is therefore done in an iterative manner by following the time integrations of the dissipative equation (17) and recalculating the thermal average from equation (50) at each time step. A self-consistent static equilibrium solution emerges after sufficient time.

As the temperature is increased, the local effective fields are reduced, thereby also changing the shape of a potential well governing the stability of a particular magnetic configuration. A de-stabilizing of the exchange bias can result with irreversible transitions between magnetic configurations.

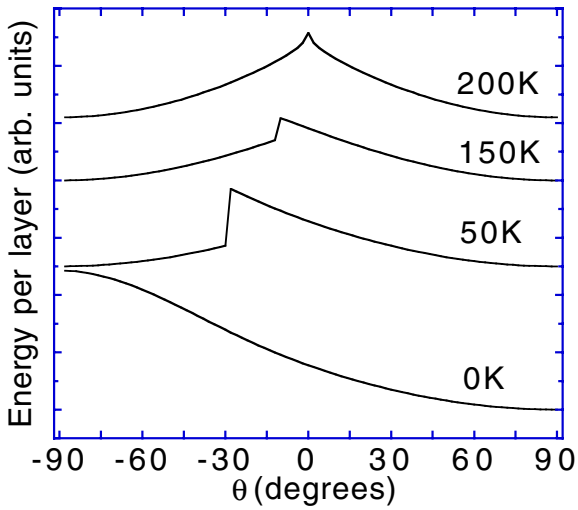


**Figure 20.** Energy of the antiferromagnet at different temperatures as a function of ferromagnet orientation. The interface is compensated and the interlayer exchange is large enough to support reversible exchange bias at zero temperature. At $T = 0$, the minimum of energy configuration is for the ferromagnet to be perpendicular to the antiferromagnet easy axis at $\theta = 90^\circ$ (Kim *et al* 1999).

This process is illustrated in figure 20 by plotting the energy of the antiferromagnet as a function of the ferromagnet orientation at different temperatures. The interface is compensated, and the interlayer exchange is chosen such that a reversible exchange bias is possible at $T = 0$. The equilibrium orientation of the ferromagnet is along the $\theta = +90^\circ$ direction, corresponding to the minimum in the antiferromagnet energy. As temperature is increased, a discontinuity in the energy appears as the ferromagnet is rotated away from the $\theta = 90^\circ$ direction. The discontinuity signals the instability of the configuration and a change into a stable configuration. The process is irreversible, and the resulting hysteresis loop is symmetric without exchange bias.

This result was found for numerical studies of compensated and uncompensated interfaces, and is a general feature of increasing temperature. As the temperature is increased, the angle at which the discontinuity appears moves closer to the $\theta = 90^\circ$ direction. This means that at low temperatures, the instability will not appear until the ferromagnet is rotated through large angles by a strong applied field. At high temperatures, the instability will occur at a smaller applied field strength. Therefore, the coercivity decreases with increasing temperature and the hysteresis loop narrows.

### 5.2. Time dependence and viscosity

As pointed out in section 3, the bias effect can appear as a purely reversible magnetization process or, in the case of partially compensated interfaces, as asymmetric hysteresis. There is another component to the problem as well. Thermal processes can lead to changes in the magnetic configurations by overcoming energy barriers. There is a probability that such an event will occur in a finite time. The probability of

an event depends on the barrier energy and the temperature of the magnetic structure.

Time-dependent effects at finite temperatures can be explored using Monte Carlo simulations (Lyberatos *et al* 1996). A model system suitable for this type of approach is based on the configuration energy in equation (13) and the barrier energy given in equation (15) (Stamps 2000). The simulation is carried out on a set of $N$ 'grains' where each grain is a ferromagnet/antiferromagnet bilayer within which the magnetizations are free to rotate in directions specified by $\theta, \alpha$ and $\psi$, but do not otherwise form domains. The grains therefore represent single domain particles large enough to support partial walls, but too small to support multi-domain structures.

The equilibrium configuration of each grain is determined for a given direction and magnitude of an external applied field using a relaxation method similar in spirit to that discussed in section 3. Because thermal fluctuations are included explicitly, it is only necessary to use the dissipative terms rather than the full Landau–Lifshitz form. The equilibrium configurations are then found by numerically integrating

$$\frac{\mathrm{d}\boldsymbol{f}}{\mathrm{d}t} = \lambda \boldsymbol{f} \times \boldsymbol{f} \times \boldsymbol{H}_{\mathrm{f}} \tag{51}$$

and

$$\frac{\mathrm{d}\boldsymbol{a}}{\mathrm{d}t} = \lambda \boldsymbol{a} \times \boldsymbol{a} \times \boldsymbol{H}_{\mathrm{a}}. \tag{52}$$

After sufficient time, the resulting configuration ceases to change and satisfies the requirement that the torques, given by equations (11) and (12), vanish. This approach appears to be stable and computationally fast, thereby allowing a large number of grains to be considered for purposes of averaging. A Metropolis algorithm is implemented in a form suitable for defining the number of events occurring in a time interval $\Delta t$.

An 'event' is here defined as an irreversible change in the magnetic configuration of a grain. As shown in the analysis of energy surfaces in section 3, at most only two configurations are possible. These correspond to partial walls in the antiferromagnet that rotate $\boldsymbol{a}$ clockwise away from the anisotropy axis, and partial walls that rotate $\boldsymbol{a}$ counterclockwise from the anisotropy axis. The irreversible event is a change from one type of partial wall to the other, achieved when a thermal fluctuation has an energy equal to or greater than the barrier energy $E_{\mathrm{b}}$ of equation (15). Suppose that a grain is at equilibrium with a particular value of $\theta$ and $\alpha$. An event is defined by letting $\alpha \rightarrow \alpha + \pi$ in $E_{\mathrm{b}}$ and finding the new values of $\theta$ and $\alpha$ consistent with this new configuration.

The number of such events occurring in time $\Delta t$ is assumed to follow the distribution

$$n(t) = \frac{N}{\tau} \exp\left[-\frac{N\Delta t}{\tau} \exp\left(-\frac{E_{\mathrm{b}}}{k_{\mathrm{B}}T}\right)\right]. \tag{53}$$

The new parameter in equation (53) is $\tau$, the relaxation time associated with the reversal. Time dependence can then be studied using standard Monte Carlo simulations with equation (53) as the acceptance probability where each Monte Carlo step corresponds to one $\Delta t$.

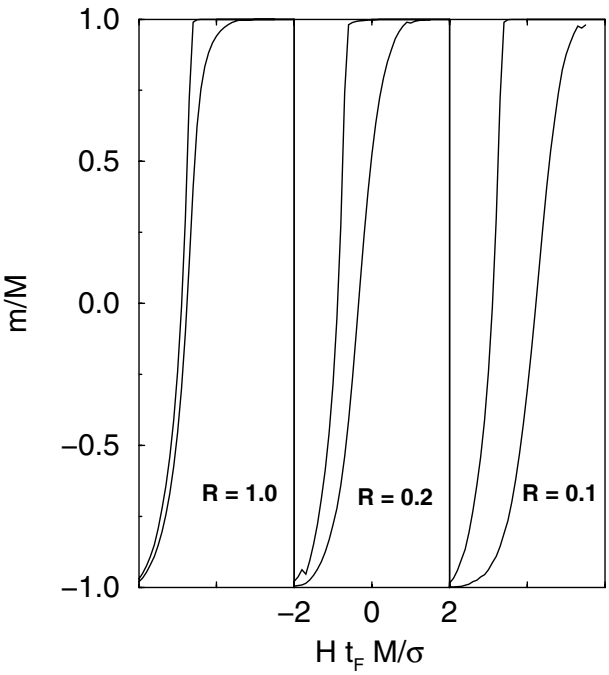


**Figure 21.** Magnetic hysteresis as a function of rate. Hysteresis loops calculated using a Monte Carlo method are shown for different rates of change $R$ of the applied field. Coercivities develop according to the rate at which the field is changed. The loops widen as the rate is reduced because there is more time for thermal activated events in the antiferromagnet to cause irreversible changes (Stamps 2000).

An interesting experiment is to examine the approach to equilibrium by varying the rate at which the magnetization loops are taken. This was done recently in experiments by Goodman *et al* (1999, 2000), with results similar to those described below. An example of the numerical results is shown in figure 21 where hysteresis is plotted for three different rates of change of the applied field.

The field was changed at each time step in these simulations at a rate $R = HMt_{\mathrm{f}}/\sigma \cdot \Delta t$. The initial configuration in each case was defined by saturating all grains with a field at $HMt_{\mathrm{f}} = 2\sigma$ in the positive direction and allowing the simulation to run until equilibrium was reached. The field was then cycled at rate $R$ in order to produce the curves shown in the figure. If the rate is large, so that the time steps between extreme field values is small, the number of thermally driven events is also small. This means that the hysteresis loop will be narrow. As the rate is reduced, meaning more time for a loop, a larger number of events occurs. The hysteresis therefore widens with decreasing rate.

The most interesting feature of these hysteresis curves is that the initial backward process is independent of rate as the field is reduced on the initial reverse path. The reason is that the grains are initially at equilibrium, and this equilibrium is independent of applied field until the ferromagnet rotates. The applied field only affects the antiferromagnet by reorientating the ferromagnet, so no events occur until the magnetization begins reversal. This explanation is consistent with the interpretation by Goodman *et al* (2000), of observed features along points on the hysteresis curve. The time during which the magnetization is

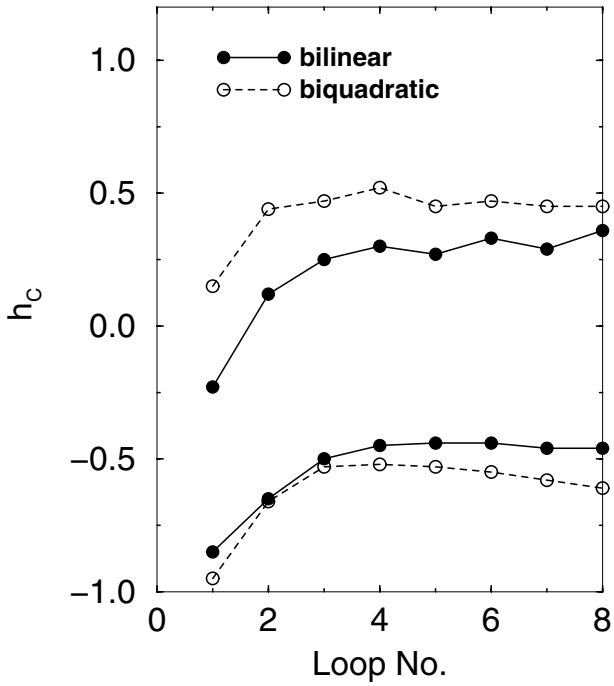


**Figure 22.** Coercive fields as a function of loop number for a sequence of hysteresis loops. Results are shown for an uncompensated interface, where the bilinear $J_1$ term dominates, and for a compensated interface where the biquadratic $J_2$ term dominates. The bias field decreases overall, and limiting values for the bias and coercive fields are reached with repeated cycling (Stamps 2000).

reversing and reversed is the time during which events leading to hysteresis can occur.

If instead a different experiment is carried out in which the field is cycled continuously, then both coercive fields defining the loop boundaries will change. This is illustrated in figure 22 where coercive fields from a sequence of loops are shown. The loop number is shown on the horizontal axis. The solid curves represent an uncompensated interface (where the $J_1$ term dominates) and the dashed curves represent a compensated interface (where the $J_2$ term dominates). The field rate is constant during each loop with magnitude $R = 0.2$. The tendency is to reduce the bias field magnitude, and also both coercive fields reduce in magnitude. The coercivity decreases quickly at first, and reach limiting values that depend upon temperature and field rate $R$.

It should be stressed that the coercivity in these simulations is due entirely to irreversible processes in the antiferromagnet. This is an interesting observation because it means that, in principle, it may be possible to use the ferromagnet component of exchange bias materials to observe magnetization processes in the antiferromagnet. In this regard, the above rate dependent effects are caused by magnetic viscosity in the antiferromagnet (Fulcomer and Charap 1972, van der Heijden *et al* 1998a). The magnetization at a reversed field changes according to the distribution in equation (53) and a viscosity parameter can be defined in terms of the time rate of change of the magnetization. The phenomena of anomalous viscosity, where the slope of the magnetization versus time curve changes sign, may arise in systems with competing intergrain exchange and magnetostatic energies (Geoghegan *et al* 1998, Stamps 2000).

It is useful to note the differences between the thermal behaviour described by the fluctuation mechanism and mean field theory. In the mean field calculations, the coercivity decreases with increasing temperature and is appropriate for low-temperature processes on timescales where large fluctuations do not occur. The thermal activation model shows an initial increase in the coercivity measured through field rate dependence and represents processes that occur as the system approaches equilibrium. This behaviour can be expected for higher temperatures where large fluctuations are likely to occur in measurable times. Furthermore, the existence of distributions of energy barriers, to both in-plane and out-of-plane fluctuations, are important in determining the long time behaviour of the viscosity and in determining effects of interaction between grains.

Finally, an important observation is that the temperature dependence of the bias and coercive fields can be different even though similar wall pinning and de-pinning mechanisms are involved. This means that coercivity can exist at temperatures where the bias field cannot, and may even be enhanced at temperatures for which bias is suppressed (Wee and Stamps 2001).

## 6. Studies of linear dynamics

Competition between interlayer exchange coupling and anisotropies determines the mechanisms responsible for exchange bias. In this regard, experimental measurements of uniaxial and easy plane anisotropies associated with the antiferromagnet and interface would be very useful.

Linear response experiments, such as ferromagnetic resonance or Brillouin light scattering, have been used with great success to identify and measure interface and surface anisotropies and interlayer exchange in multilayer systems (Hillebrands and Güntherodt 1994). In a calculation of spin wave frequencies, Stamps *et al* (1996) argued that these same techniques applied to exchange coupled bilayers can provide quantitative measures of the easy plane and uniaxial anisotropies in an antiferromagnet.

The reason is that the frequencies of long wavelength spin wave modes are sensitive to components of the local internal magnetic fields associated with small deviations of the magnetization from equilibrium. The internal fields at the interfaces can be different from those inside the films, and it is often possible to identify effects of interface and surface local fields through frequency measurements.

The exchange bias structure is particularly nice to study because frequencies associated with spin waves in the ferromagnet can be readily measured. Interface driven changes in the spin wave frequencies can be studied and related to interlayer exchange and anisotropy parameters associated with the antiferromagnet. Because an antiferromagnet such as CoO has a lower ordering temperature than ferromagnetic Co, thermal effects can be used to help identify the antiferromagnet contributions to the frequencies.

This technique was used by Ercole *et al* (2000) on Co/CoO bilayers in a light scattering study of exchange bias.

Other studies have been made by Mathieu *et al* (1998) on Permalloy/FeMn multilayers, in an investigation of angular dependence of bias on field orientation. Ferromagnetic resonance experiments provide similar information, and have been carried out by several groups on a variety of exchange coupled systems (Stoecklein *et al* 1988, Krebs *et al* 1993, McMichael *et al* 1998, Rubinstein *et al* 1999).

This technique is not limited to bilayers. Calculations of linear response for magnetic trilayers consisting of an exchange coupled ferromagnet/antiferromagnet/ferromagnet show that it is possible to distinguish between different forms of interlayer exchange coupling mechanisms (Chirita *et al* 1998). Proposed forms for interlayer exchange include that of equation (13), and a form suggested by Slonczewski (1991) for a mixed interface:

$$E_{\text{inter}} = C_+(\theta_1 - \theta_2)^2. \tag{54}$$

The two angles specify the orientations of the magnetizations in the separate films. The effects of this energy on spin wave frequencies is dramatically different from that of equation (13) when frequencies are measured as a function of applied field. It is also noted that experiments and calculations on magnetization properties of similar trilayer structures have been reported (Filipkowski *et al* 1995, Xi and White 2000b) in which this type of coupling was considered.

## 7. Summary and conclusions

The problem of exchange bias is interesting and important because in order to understand it fully one must understand some of the most difficult issues basic to magnetism. These issues include questions of magnetic ordering in frustrated systems, exchange interactions and correlations at interfaces, and disorder and impurity effects at the interface.

One of the themes outlined in this article was the problem of magnetic order and magnetization processes at less than perfect interfaces. It has been argued that the magnetic and thermal stability of magnetic configurations formed on either side of the interface control the appearance of exchange bias shifts in magnetization measurements. A consequence is that two different types of exchange bias may exist: one in which the process is the reversible formation of partial walls, and the other whereby asymmetric hysteresis loops are produced by irreversible processes. The formation of asymmetric hysteresis can occur without complete loss of partial wall reversible bias if the interfaces are mixed, and result in shifted and asymmetric loops.

A tool for characterizing exchange bias at mixed and geometrically rough interfaces is the concept of a natural angle. Determination of the natural angle provides a measure directly related to the degree by which the antiferromagnet sublattices are mixed at the interface. This also has consequences on the magnitude and type of effective exchange field acting on the ferromagnet. A direct relationship exists between the natural angle, the bilinear and biquadratic exchange energies, and the amount of each sublattice present at the interface.

The behaviour with temperature is particularly important with regards to stability of the exchange bias. Mean field calculations show that coercive fields and the exchange bias field decrease with increasing temperature. A fluctuation theory of thermal activation over energy barriers allows a description of the rate at which equilibrium is approached. The approach to equilibrium can be studied with field rate experiments, in which an initial increase in coercivity simultaneous with a decrease in exchange bias field is predicted and observed. The timescales on which this happens depend on the barriers to thermal activation. These are partly determined by the exchange parameters, magnetostatic interaction energies in the ferromagnet, wall and anisotropy energies in the ferromagnet and antiferromagnet, and interface and out-of-plane anisotropies in the antiferromagnet. A consequence is that measurements of the exchange bias can be sensitive to the method of measurement, with particular dependence on the timescales involved (Xi *et al* 1999b, Goodman *et al* 1999, 2000, Stamps 2000).

The magnetic configuration within a domain wall length of the interface determines the bias field and coercivity in the micromagnetic mechanisms described here. The type of configuration possible at different temperatures is sensitive to the geometry of the interface region, and several features of exchange bias and coercivity can be controlled by introducing structure at the interface. Exchange bias in small particles and grains composed of ferromagnetic and antiferromagnetic materials are particularly sensitive to geometry. Film thicknesses, grain sizes and particle dimensions of the order of domain wall lengths can prohibit or destabilize partial wall formation and increase sensitivity to thermal fluctuations. A consequence is that control of the magnetization history can be used to modify the bias and coercivity (Miltényi *et al* 1999, Nogués *et al* 2000b). An extreme example is the observation of positive exchange bias shifts, understood in terms of cooling in applied fields large enough to saturate the antiferromagnet in its paramagnetic phase (Nogués *et al* 1996, 2000a).

Finally, a particularly fascinating aspect is the question of how domain wall motion and nucleation affect coercivity in ferromagnet/antiferromagnet heterostructures. The partial wall formation and stability issues discussed in previous sections are concerned primarily with wall pinning to the interface. Pinning mechanisms against domain wall motion along the interface also exist (Dantas and Carriço 1998). There is also the possibility of self-pinning of walls in exchange coupled films, with associated energies and dynamics resonances (Stamps *et al* 1997, Dantas *et al* 2001). The additional complexity and novel features of the exchange coupled interface make the problem of domain wall nucleation and dynamics particularly rich.

## Acknowledgments

The author acknowledges support under the Australian Research Council for this work. Special thanks are given to J-V Kim, L Wee and R E Camley for stimulating and productive collaborations on a variety of problems relating to exchange bias. Thanks are given to A Carriço, R Chantrell, H Danan, A Dantas, A Ercole, J Fassbender, R Hicken, B Hillebrands, T Mewes, J Nogués, K O'Grady, S Parkin,

C Patton and R Street for useful and illuminating discussions. The author is particularly grateful to J Krebs and R E Camley for providing motivation and inspiring interest in this topic.

## References


Allegranza O and Chen M-M 1993 Effect of substrate and antiferromagnetic film's thickness on exchange-bias field *J. Appl. Phys.* **73** 6218–22

Ambrose T and Chien C L 1994 Magnetic properties of exchange coupled NiFe/CoO/NiFe trilayers *Appl. Phys. Lett.* **65** 1967–9

Ambrose T, Sommer R L and Chien C L 1997 Angular dependence of exchange coupling in ferromagnet/antiferromagnet bilayers *Phys. Rev.* B **56** 83–6

Berkowitz A E and Takano K 1999 Exchange anisotropy—a review *J. Magn. Magn. Mater.* **200** 552–70

Camley R E, McGrath B V, Astalos R J, Stamps R L, Kim J-V and Wee L 1999 Magnetization dynamics: A study of the ferromagnet/antiferromagnet interface and exchange biasing *J. Vac. Sci. Technol.* A **17** 1335–9

Carrico A S, Camley R E and Stamps R L 1994 Phase diagram of thin antiferromagnetic films in strong magnetic fields *Phys. Rev.* B **50** 13 453–60

Chirita M, Robins G, Stamps R L, Sooryakumar R, Filipkowski M E, Gutierrez C J and Prinz G A 1998 Brillouin light scattering study of magnetic coupling in CoFe/Mn/CoFe *Phys. Rev.* B **58** 869–75

Chopra H D, Yang D X, Chen P J, Brown H J, Swartzendruber L J and Egelhoff W F 2000 Nature of magnetization reversal in exchange-coupled polycrystalline NiO–Co bilayers *Phys. Rev.* B **61** 15 312–20

Dantas A L and Carriço A S 1998 *J. Phys.: Condens. Matter* **11** 3792

Dantas A L, Carriço A S and Stamps R L 2001 Local modes of thin magnetic films *Phys. Rev.* B **62** 8650–3

Dimitrov D V, Zhang S, Xiao J Q, Hadjipanayis G C and Prados C 1998 Effect of exchange interactions at antiferromagnetic/ferromagnetic interfaces *Phys. Rev.* B **58** 12 090–4

Ercole A, Lew W S, Lauhoff G, Kernohan E T M, Lee J and Bland J A C 2000 Temperature-dependent spin-wave behaviour in Co/CoO bilayers studied by Brillouin light scattering *Phys. Rev.* B **62** 6429–36

Escorcia-Aparicio E J 1998 90° magnetization switching in thin Fe films grown on stepped Cr(001) *Phys. Rev. Lett.* **81** 2144–7

Farrow R F C, Marks R F, Gider S, Marley A C, Parkin S S P and Mauri D 1997 $Mn_xPt_{1-x}$: A new exchange bias material for Permalloy *J. Appl. Phys.* **81** 4986–8

Filipkowski M E, Krebs J J, Prinz G A and Gutierrez C J 1995 *Phys. Rev. Lett.* **75** 1847

Fitzsimmons M R, Yashar P, Leighton C, Schuller I K, Nogués J, Majkrzak C F and Dura J A 2000 Asymmetric magnetization reversal in exchange-biased hysteresis loops *Phys. Rev. Lett.* **84** 3986–9

Fulcomer E and Charap S H 1972 Thermal fluctuation after-effect model for some systems with ferromagnetic–antiferromagnetic coupling *J. Appl. Phys.* **43** 4190–9

Geoghegan D S, McCormick P G and Street R 1998 *J. Magn. Magn. Mater.* **177** 937

Gökemeijer N J, Cai J W and Chien C L 1999 Memory effects of exchange coupling in ferromagnet/antiferromagnet bilayers *Phys. Rev.* B **60** 3033–6

Goodman A M, Laider H, O'Grady K, Owen N W and Petford-Long A K 2000 Magnetic viscosity effects on the pinned layer of spin-valve materials *J. Appl. Phys.* **87** 6409–11

Goodman A M, O'Grady K, Parker M R and Burkett S 1999 Competing sweep-rate dependent effects in the hard loop of spin-valve multilayers *J. Magn. Magn. Mater.* **193** 504

Hillebrands B and Güntherodt G 1994 Brillouin light scattering in magnetic superlattices *Ultrathin Magnetic Structures II* ed J A C Bland (Berlin: Springer)

Hong T M 1998 Simple mechanism for a positive exchange bias *Phys. Rev.* B **58** 97–100

Jacobs I S and Bean C P 1966 Fine Particles, Thin Films and Exchange Anisotropy (Effects of Finite Dimensions and Interfaces on the Basic Properties of Ferromagnets) ch 6 *Magnetism* vol III, ed H Suhl, pp 271–350

Jiang J S, Felcher G P, Inomata A, Goyette R, Nelson C and Bader S D 2000 Exchange-bias effect in Fe/Cr(211) double superlattice structures *Phys. Rev.* B **61** 9653–6

Ju G, Nurmikko A V, Farrow R F C, Marks R F, Carey M J and Gurney B A 1999 Ultrafast time resolved photoinduced magnetization rotation in a ferromagnetic/antiferromagnetic exchange coupled system *Phys. Rev. Lett.* **82** 3705–8

Kim J-V and Stamps R L 2001 unpublished

Kim J-V, Stamps R L, McGrath B V and Camley R E 2000 Angular dependence and interfacial roughness in exchange-biased ferromagnetic/antiferromagnetic bilayers *Phys. Rev.* B **61** 8888–94

Kim J-V, Wee L, Stamps R L and Street R 1999 Exchange bias: Interface imperfections and temperature dependence *IEEE Trans. Magn.* **35** 2994–7

Kiwi M, Mejía-López J, Portugal R D and Ramírez R 1999a Exchange bias model for $Fe/FeF_2$: Role of domains in the ferromagnet *Europhys. Lett.* **48** 573–9

Kiwi M, Mejía-López J, Portugal R D and Ramírez R 1999b Exchange-bias systems with compensated interfaces *Appl. Phys. Lett.* **75** 3995–7

Koon N C 1997 Calculations of exchange bias in thin films with ferromagnetic/antiferromagnetic interfaces *Phys. Rev. Lett.* **78** 4865–8

Kouvel J S 1963 A ferromagnetic–antiferromagnetic model for copper–manganese and related alloys *J. Phys. Chem. Solids* **24** 795–822

Krebs J J, Lind D M and Berry S D 1993 Ferromagnetic resonance and spin anisotropy in iron oxide thin films and iron oxide/nickle oxide superlattices *J. Appl. Phys.* **73** 6457–9

Lederman D, Nogués J and Schuller I K 1997 Exchange anisotropy and the antiferromagnetic surface order parameter *Phys. Rev.* B **56** 2332–5

Leighton C, Nogués J, Jönsson-Åkerman B and Schuller I K 2000 Coercivity enhancement in exchange biased systems driven by interfacial magnetic frustration *Phys. Rev. Lett.* **84** 3466–9

Li Z and Zhang S 2000 Magnetization reversal of ferromagnetic/antiferromagnetic bilayers *Appl. Phys. Lett.* **77** 423–5

Lyberatos A, Earl J and Chantrell R W 1996 *Phys. Rev.* B **53** 5493

Malozemoff A P 1987 Random-field model of exchange anisotropy at rough ferromagnetic–antiferromagnetic interfaces *Phys. Rev.* B **35** 3679–82

Malozemoff A P 1988 Heisenberg-to-Ising crossover in a random-field model with uniaxial anisotropy *Phys. Rev.* B **37** 7673–9

Mathieu C, Bauer M, Hillebrands B, Fassbender J, Güntherodt G, Jungblut R, Kohlhepp J and Reinders A 1998 Brillouin light scattering investigations of exchange biased (110)-oriented NiFe/FeMn bilayers *J. Appl. Phys.* **83** 2863–5

Mauri D, Siegmann H C, Bagus P S and Kay E 1987 Simple model for thin ferromagnetic films exchange coupled to an antiferromagnetic substrate *J. Appl. Phys.* **62** 3047–9

McGrath B V and Camley R E 2000 Temperature dependence of exchange biased thin films *J. Appl. Phys.* **87** 1–3

McMichael R D, Stiles M D, Chen P J and Egelhoff W F 1998 Ferromagnetic resonance studies of NiO-coupled thin films of Ni(80)Fe(20) *Phys. Rev.* B **58** 8605–11

Meiklejohn W H 1962 Exchange anisotropy—a review *J. Appl. Phys.* **33** S1328–9

Meiklejohn W H and Bean C P 1956 New magnetic anisotropy (Letter) *Phys. Rev.* **102** 1413–4

Meiklejohn W H and Bean C P 1957 New magnetic anisotropy

*Phys. Rev.* **105** 904–13
Mewes T, Lopusnik R, Fassbender J, Hillebrands B, Jung M, Engel D, Ehresmann A and Schmoranzer H 2000 Suppression of exchange bias by ion irradiation *Appl. Phys. Lett.* **76** 1057–9
Miltényi P, Gierlings M, Bamming M, May U, Güntherodt G, Nogués J, Gruyters M, Leighton C and Schuller I K 1999 Tuning exchange bias *Appl. Phys. Lett.* **75** 2304–6
Miltényi P, Gierlings M, Keller J, Beschoten B, Güntherodt G, Nowak U and Usadel K D 2000 Diluted antiferromagnets in exchange bias: proof of the domain state model *Phys. Rev. Lett.* **84** 4224–7
Néel L 1967 Etude théorique du couplage ferro–antiferromagnétique dans les couches minces *Ann. Phys., Paris* **2** 61–80
Néel L 1988 *A Theoretical Study of the Ferro–Antiferromagnetic Coupling between Thin Films* pp 469–87
Nemoto A, Otani Y, Kim S G, Fukamichi K, Kitakami O and Shimada Y 1999 Magnetoresistance and planar hall effects in submicron exchange-coupled NiO/$Fe_{19}Ni_{81}$ wires *Appl. Phys. Lett.* **74** 4026–8
Nikitenko V I, Gornakov V S, Dedukh L M, Kabanov Y P, Khapikov A F, Shapiro A J, Shull R D, Chaiken A and Michel R P 1998 Asymmetry of domain nucleation and enhanced coercivity in exchange-biased epitaxial NiO/NiFe bilayers *Phys. Rev.* B **57** R8111–4
Nikitenko V I, Gornakov V S, Shapiro A J, Shull R D, Liu K, Zhou S M and Chien C L 2000 Asymmetry in elementary events of magnetization reversal in a ferromagnetic/antiferromagnetic bilayer *Phys. Rev. Lett.* **84** 765–8
Nogués J, Lederman D, Moran T J and Schuller I K 1996 Positive exchange bias in FeF(2)–Fe bilayers *Phys. Rev. Lett.* **76** 4624–7
Nogués J, Leighton C and Schuller I K 2000a Correlation between antiferromagnetic interface coupling and positive exchange bias *Phys. Rev.* B **61** 1315–7
Nogués J, Moran T J, Lederman D, Schuller I K and Rao K V 1999 Role of interfacial structure on exchange-biased FeF(2)–Fe *Phys. Rev.* B **59** 6984–93
Nogués J, Morellon L, Leighton C, Ibarra M R and Schuller I K 2000b Antiferromagnetic spin flop and exchange bias *Phys. Rev.* B **61** R6455–8
Prinz G 1995 Spin-polarized transport *Phys. Today* **48** 58–63
Rubinstein M, Lubitz P and Cheng S-F 1999 Ferromagnetic-resonance field shift in an exchange-biased CoO/$Ni_{80}Fe_{20}$ bilayer *J. Magn. Magn. Mater.* **195** 299–306
Schlenker C 1968a *Phys. Status Solidi* **28** 507
Schlenker C 1968b Couplage ferro–antiferromagnetique et traĩnage magnétique dans des couches minces multiples Co–CoO et Ni–NiO *Phys. Status Solidi* **28** 507–17
Schlenker C and Paccard D 1967 *J. Phys.* **28** 611
Schlenker C, Parkin S S P, Scott J C and Howard K 1986 Magnetic disorder in the exchange bias bilayered FeNi–FeMn system *J. Magn. Magn. Mater.* **54** 801–2
Schulthess T C and Butler W H 1998 Consequences of spin-flop coupling in exchange biased films *Phys. Rev. Lett.* **81** 4516–9
Schulthess T C and Butler W H 1999 Coupling mechanisms in exchange biased films *J. Appl. Phys.* **85** 5510–5
Slonczewski J C 1991 Fluctuation mechanism for biquadratic exchange coupling in magnetic multilayers *Phys. Rev. Lett.* **67** 3172–5
Sort J, Nogués J, Amils X, Suriñach S, Muñoz J S and Báro M D 1999 Room-temperature coercivity enhancement in mechanically alloyed antiferromagnetic–ferromagnetic powders *Appl. Phys. Lett.* **75** 3177–9
Stamps R L 2000 Dynamic magnetic hysteresis and anomalous viscosity in exchange bias systems *Phys. Rev.* B **61** 12 174–80
Stamps R L, Camley R E and Hicken R J 1996 Influence of exchange-coupled anisotropies on spin-wave frequencies in magnetic layered systems: application to Co/CoO *Phys. Rev.* B **54** 4159–64
Stamps R L, Carriço A S and Wigen P E 1997 Domain wall waves in coupled films *Phys. Rev.* B **55** 6473–84
Stiles M D and McMichael R D 1999a Model for exchange bias in polycrystalline ferromagnet–antiferromagnet bilayers *Phys. Rev.* B **59** 3722–33
Stiles M D and McMichael R D 1999b Temperature dependence of exchange bias in polycrystalline ferromagnet–antiferromagnet bilayers *Phys. Rev.* B **60** 12 950–6
Stoecklein W, Parkin S S P and Scott J C 1988 Ferromagnetic resonance studies of exchange-biased Permalloy thin films *Phys. Rev.* B **38** 6847–54
Suhl H and Schuller I K 1998 Spin-wave theory of exchange-induced anisotropy *Phys. Rev.* B **58** 258–64
Tang Y J, Roos B, Mewes T, Demotrikov S O, Hillebrands B and Wang Y J 1999 Enhanced coercivity of exchange-bias Fe/MnPd bilayers *Appl. Phys. Lett.* **75** 707–9
Tsunoda M, Tsuchiya Y, Hashimoto T and Takahashi M 2000 Magnetic anisotropy and rotational hysteresis loss in exchange coupled Ni–Fe/Mn–Ir films *J. Appl. Phys.* **87** 4375–88
Uyama H, Otani Y, Fukamichi K, Kitakami O, Shimada Y and Echigoya J 1997 Effect of antiferromagnetic grain size on exchange-coupling field of $Cr_{70}Al_{30}$/$Fe_{19}Ni_{81}$ bilayers *Appl. Phys. Lett.* **71** 1258–60
van der Heijden P A A, Maas T F M M, de Jonge W J M, Kools J C S, Roozeboom F and van der Zaag P J 1998a Thermally assisted reversal of exchange biasing in NiO and FeMn based systems *Appl. Phys. Lett.* **72** 492–4
van der Heijden P A A, Maas T F M M, Kools J C S, Roozeboom F, van der Zaag P J and de Jonge W J M 1998b Influences on relaxation of exchange biasing in NiO/$Ni_{66}Co_{18}Fe_{16}$ bilayers *J. Appl. Phys.* **83** 7207–9
van Driel J, de Boer F R, Lenssen K-M H and Coehoorn R 2000 Exchange biasing by Ir(19)Mn(81): Dependence on temperature, microstructure and antiferromagnetic layer thickness *J. Appl. Phys.* **88** 975–82
Wee L and Stamps R L 2001 unpublished
Wu X W and Chien C L 1998 Exchange coupling in ferromagnet/antiferromagnet bilayers with comparable $T$(C) and $T$(N) *Phys. Rev. Lett.* **81** 2795–8
Xi H, Kryder M H and White R M 1999a Study of the angular-dependent exchange coupling between a ferromagnetic and an antiferromagnetic layer *Appl. Phys. Lett.* **74** 2687–9
Xi H and White R M 1999 Angular dependence of exchange anisotropy in $Ni_{81}Fe_{19}$/CrMn$Pt_x$ bilayers *J. Appl. Phys.* **86** 5169–74
Xi H and White R M 2000a Antiferromagnetic thickness dependence of exchange biasing *Phys. Rev.* B **61** 80–3
Xi H and White R M 2000b Coupling between two ferromagnetic layers separated by an antiferromagnetic layer *Phys. Rev.* B **62** 3933–40
Xi H, White R M and Rezende S M 1999b Irreversible and reversible measurements of exchange anisotropy *Phys. Rev.* B **60** 14 837–40